References

1) Hortobágyi G. N., *Drugs*, **54** (Suppl. 4), 1—7 (1997).
2) Di Marco A., Gaetani M., Scarpinato B., *Cancer Chemother. Rep.*, **53**, 33—37 (1969).
3) O'Brien M. E., Wigler N., Inbar M., Rosso R., Grischke E., Santoro A., Catane R., Kieback D. G., Tomczak P., Ackland S. P., Orlandi F., Mellars L., Alland L., Tendler C., CAELYX Breast Cancer Study Group, *Ann. Oncol.*, **15**, 440—449 (2004).
4) Olson R. D., Mushlin P. S., Brenner D. E., Fleischer S., Cusack B. J., Chang B. K., Boucek R. J. Jr., *Proc. Natl. Acad. Sci. U.S.A.*, **85**, 3585—3589 (1988).
5) van Asperen J., van Tellingen O., Beijnen J. H., *Drug Metab. Dispos.*, **28**, 264—267 (2000).
6) Yokoyama M., Okano T., Sakurai Y., Fukushima S., Okamoto K., Kataoka K., *J. Drug Target.*, **7**, 171—186 (1999).
7) Nakanishi T., Fukushima S., Okamoto K., Suzuki M., Matsumura Y., Yokoyama M., Okano T., Sakurai Y., Kataoka K., *J. Controlled Release*, **74**, 295—302 (2001).
8) Sakai-Kato K., Saito E., Ishikura K., Kawanishi T., *J. Chromatogr. B Analyt. Technol. Biomed. Life Sci.*, **878**, 1466—1470 (2010).
9) Swartz M. E., *J. Liq. Chrom. Rel. Technol.*, **28**, 1253—1263 (2005).
10) Nováková L., Vlcková H., *Anal. Chim. Acta*, **656**, 8—35 (2009).
11) Sun N., Lu G., Lin M., Fan G., Wu Y., *Talanta*, **78**, 506—512 (2009).
12) van Asperen J., van Tellingen O., Beijnen J. H., *J. Chromatogr. B Biomed. Sci. Appl.*, **712**, 129—143 (1998).
13) Zhou Q., Chowbay B., *J. Pharm. Biomed. Anal.*, **30**, 1063—1074 (2002).
14) Maudens K. E., Stove C. P., Lambert W. E., *J. Sep. Sci.*, **31**, 1042—1049 (2008).
15) Takanashi S., Bachur N. R., *Drug Metab. Dispos.*, **4**, 79—87 (1976).
16) Andersen A., Warren D. J., Slørdal L., *Ther. Drug Monit.*, **15**, 455—461 (1993).
17) Shinozawa S., Mimaki Y., Araki Y., Oda T., *J. Chromatogr.*, **196**, 463—469 (1980).
18) Rose L. M., Tillery K. F., el Dareer S. M., Hill D. L., *J. Chromatogr.*, **425**, 419—423 (1988).
19) Andersen A., Holte H., Slørdal L., *Cancer Chemother. Pharmacol.*, **44**, 422—426 (1999).
20) Guidance for Industry: Bioanalytical Method Validation. U.S. Department of Health and Human Services Food and Drug Administration (2001)
21) Lown J. W., *Pharmacol. Ther.*, **60**, 185—214 (1993).
22) van Asperen J., van Tellingen O., Tijssen F., Schinkel A. H., Beijnen J. H., *Br. J. Cancer*, **79**, 108—113 (1999).

International Journal of Pharmaceutics 423 (2012) 401–409

Contents lists available at SciVerse ScienceDirect

International Journal of Pharmaceutics

journal homepage: www.elsevier.com/locate/ijpharm

Pharmaceutical nanotechnology

Evaluation of intracellular trafficking and clearance from HeLa cells of doxorubicin-bound block copolymers

Kumiko Sakai-Kato[a,*], Keiko Ishikura[a], Yuki Oshima[a], Minoru Tada[b], Takuo Suzuki[b], Akiko Ishii-Watabe[b], Teruhide Yamaguchi[c], Nobuhiro Nishiyama[d], Kazunori Kataoka[d,e], Toru Kawanishi[c], Haruhiro Okuda[a]

[a] Division of Drugs, National Institute of Health Sciences, 1-18-1 Kamiyoga, Setagaya-ku, Tokyo 158-8501, Japan
[b] Division of Biological Chemistry and Biologicals, National Institute of Health Sciences, 1-18-1 Kamiyoga, Setagaya-ku, Tokyo 158-8501, Japan
[c] National Institute of Health Sciences, 1-18-1 Kamiyoga, Setagaya-ku, Tokyo 158-8501, Japan
[d] Center for Disease Biology and Integrative Medicine, Graduate School of Medicine, The University of Tokyo, 7-3-1 Hongo, Bunkyo-ku, Tokyo 113-0033, Japan
[e] Department of Materials Engineering, Graduate School of Engineering, The University of Tokyo, 7-3-1 Hongo, Bunkyo-ku, Tokyo 113-8656, Japan

ARTICLE INFO

Article history:
Received 1 July 2011
Received in revised form
16 November 2011
Accepted 15 December 2011
Available online 23 December 2011

Keywords:
Doxorubicin-bound block copolymers
Intracellular trafficking
Confocal microscopy
Transporter
Endocytosis

ABSTRACT

New technologies are needed to deliver medicines safely and effectively. Polymeric nanoparticulate carriers are one such technology under investigation. We examined the intracellular trafficking of doxorubicin-bound block copolymers quantitatively and by imaging doxorubicin-derived fluorescence using confocal microscopy. The polymers were internalized by endocytosis and distributed in endosomal/lysosomal compartments and the endoplasmic reticulum; unlike free doxorubicin, the polymers were not found in the nucleus. Moreover, the ATP-binding cassette protein B1 (ABCB1) transporter may be involved in the efflux of the polymer from cells. This drug delivery system is attractive because the endogenous transport system is used for the uptake and delivery of the artificial drug carrier to the target as well as for its efflux from cells to medium. Our results show that a drug delivery system strategy targeting this endogenous transport pathway may be useful for affecting specific molecular targets.

1. Introduction

Recently, genomic drug discovery techniques, organic synthesis, and screening technologies have been used to develop molecularly targeted medicines, some of which are already being used clinically (Hopkins and Groom, 2002; Hughes, 2009). However, these new technologies do not necessarily lead to the introduction of new treatments because even when promising compounds are discovered by genomic drug discovery techniques, they often have harmful properties or are difficult to deliver to the target because they are relatively insoluble (Hopkins and Groom, 2002; Lipinski et al., 2001). New formulation technologies are being developed to enhance the effectiveness and safety of pharmaceutical products by focusing on improving the release, targeting, and stability of drugs within the body, so that the location and timing of their action in the living body can be controlled.

Nanotechnological advances have contributed to the development of new drug delivery system (DDS) products such as polymeric micelles and liposomes that range in size from several tens of nanometers to 100 nm (Ferrari, 2005). Some of these DDS products are already being marketed as innovative medical treatments (O'Brien et al., 2004), and the number being used in clinical trials has risen impressively in recent years (Hamaguchi et al., 2007; Kuroda et al., 2009; Matsumura et al., 2004). These nanoparticulates possess several unique advantages for drug delivery, including high drug-loading capacity, controlled drug release, and small size, which allows the drug to accumulate in pathological tissues such as tumors, which have increased vascular permeability (Nishiyama and Kataoka, 2006).

Polymeric micelles have received considerable attention recently as promising macromolecular carrier systems (Allen et al., 1999; Kataoka et al., 1993, 2001; Lavasanifar et al., 2002; Torchilin, 2002; Torchilin et al., 2003). Polymeric micelles are amphipathic systems in which a hydrophobic core is covered with an outer

Abbreviations: DDS, drug delivery system; PEG, polyethyleneglycol; RES, reticuloenodothelial system; EPR, enhanced permeability and retention; Dox, doxorubicin; DMEM, Dulbecco's modified Eagle's medium; FBS, fetal bovine serum; DLS, dynamic light scattering; AFM, atomic force microscopy; HBSS, Hank's balanced salt solution; ER, endoplasmic reticulum; ECFP, enhanced cyan fluorescent protein; Alexa-transferrin, Alexa Fluor 488 conjugate of transferrin; MTOC, microtubule-organizing center; ABCB1, ATP-binding cassette protein B1; MDR1, multidrug resistance 1; (PBS), phosphate-buffered saline; EDTA, ethylenediamine tetraacetic acid; SDS, sodium dodecyl sulfate; PVDF, polyvinylidene fluoride.

* Corresponding author. Tel.: +81 3 3700 9662; fax: +81 3 3700 9662.
E-mail address: kumikato@nihs.go.jp (K. Sakai-Kato).

0378-5173/$ – see front matter © 2011 Elsevier B.V. All rights reserved.
doi:10.1016/j.ijpharm.2011.12.022

shell consisting of hydrophilic macromolecules such as polyethylene glycol (PEG) chains. Polymeric micelles can both encapsulate medicine of high density and evade the foreign body recognition mechanism within the reticuloendothelial system (RES), and they show excellent retention in the blood (Illum et al., 1987). In addition, accurate size control of the nanoparticulates enables them to accumulate in cancerous tissue, owing to the increased permeability of tumor vessels due to the enhanced permeability and retention (EPR) effect (Matsumura and Maeda, 1986).

To maximize the efficacy and safety of DDS products, it is important to deliver these products to specific target cells and subcellular compartments. In the experiments reported here, we used confocal microscopy to study the intracellular trafficking of polymeric nanoparticulate carriers. The use of covalently bound fluorescent reagents as probes is gradually clarifying the internalization pathways and intracellular localizations of polymeric nanoparticulate carriers (Lee and Kim, 2005; Manunta et al., 2007; Murakami et al., 2011; Rejman et al., 2005; Richardson et al., 2008; Sahay et al., 2008; Savić et al., 2003). However, the excretion of the polymers from target cells after they have released the incorporated drugs has not yet been clarified in detail, although information about the clearance of carriers from cells is important from the perspective of safety. In this study, we examined the trafficking of a polymeric nanoparticulate carrier in detail, including the efflux of the polymers from cells to medium, by direct measurement of doxorubicin (Dox) covalently bound to the block copolymer. This technique avoids the necessity of considering the effects of exogenously tagged fluorescent probes on the intracellular trafficking.

Dox is one of the most effective available anticancer drugs in spite of its severe toxic effects, especially cardiotoxicity (Olson et al., 1988). As the carrier we used a PEG-poly(aspartic acid) block copolymer with covalently bound Dox (Fig. 1) (Yokoyama et al., 1999), because Dox has relevant hydrophobicity to form globular micelles by means of the hydrophobic interactions, and inherent fluorescence to investigate the intracellular trafficking of the carrier itself. Dox is partially covalently bound to the side chain of the aspartic acid (about 45% of aspartic acids), so that prepared Dox-conjugated block copolymers show good Dox entrapment efficiency possibly due to the π–π interaction between conjugated and incorporated Dox molecules (Bae and Kataoka, 2009; Nakanishi et al., 2001). Therefore, in this carrier system, there are two kinds of Dox; one is Dox covalently bound to block copolymers, and the other is free Dox which is incorporated in the inner core and has a pharmacological activity by its release from the inner core. The inner core of the micelles is greatly hydrophobic owing to the conjugated Dox, while the PEG of the outer layer prevents uptake by the RES. The resulting micelle effectively accumulates in tumor tissue by the EPR effect and shows much stronger activity than free Dox (Nakanishi et al., 2001). Because the block copolymer can form globular micelles by means of hydrophobic interactions with the conjugated Dox, as shown in Section 3.1, we used a carrier without incorporated free Dox to investigate the intracellular trafficking of the carrier itself. Furthermore, by quantifying directly the amount of Dox covalently bound to the polymers, we could measure the intracellular amount of the polymers.

2. Materials and methods

2.1. Cells and micelles

HeLa cells (Health Science Research Resources Bank, Osaka, Japan) were kept in Dulbecco's modified Eagle's medium (DMEM; Invitrogen Corp., Carlsbad, CA, USA) supplemented with 10% fetal bovine serum (FBS; Nichirei Biosciences Inc., Tokyo, Japan) and 100 U/mL penicillin/streptomycin (Invitrogen). Cells were grown in a humidified incubator at 37 °C under 5% CO_2. Dox-bound polymeric micelles and fluorescent dye (DBD)-labeled PEG-polyaspartate block copolymers partially modified with 4-phenyl-1-butanol were synthesized by Nippon Kayaku Co. Ltd. (Tokyo, Japan) (Nakanishi et al., 2001).

2.2. Physicochemical data of Dox-bound micelles

The diameters and distribution of micelles were determined by using dynamic light scattering (DLS; Zetasizer Nano ZS, Malvern, UK) at 25 °C. The micelles were dissolved in water and filtered through a 0.2-μm filter before measurement. Atomic force microscopy (AFM) measurements were conducted with a NanoWizard II (JPK Instruments, Berlin, Germany) at room temperature. Images were obtained in tapping mode using a commercial microcantilever with a spring constant of 150 N/m (Olympus Corporation, Tokyo, Japan). AFM images were processed with SPM image processing v. 3 software from JPK Instruments.

2.3. Quantitation of Dox-bound polymers in HeLa cells

The amounts of Dox-bound polymers in HeLa cells were determined by measuring the amount of doxorubicinone, which is released by acid hydrolysis of Dox-bound polymers (Fig. 1b). HeLa cells (1.5×10^5) were plated in 35-mm glass-bottom dishes coated with poly-L-lysine (Matsunami, Osaka, Japan) in DMEM containing 10% FBS and 100 U/mL penicillin/streptomycin. After incubation for two days (37 °C, 5% CO_2), the cells were exposed to 50 μg/mL Dox-bound polymers in culture medium. After the indicated durations, the cells were washed and kept in phosphate-buffered saline (PBS) or Hank's balanced salt solution (HBSS; Invitrogen). The cells were trypsinized with 0.25% trypsin-ethylenediamine tetraacetic acid (EDTA) (Invitrogen) and collected. Cells were then washed with PBS three times, and a small part of the cell suspension was used for cell counting. After centrifugation at 1000 rpm for 5 min, cell pellets were resuspended in 100 μL PBS, and the suspension was divided into two parts (50 μL was used with acid hydrolysis and 50 μL without) and stored at −80 °C until analysis. After thawing, the cell suspensions were disrupted by ultrasonic liquid processor (ASTRASON 3000, Misonix, NY, USA) for 1 min. Then, 50 μL of suspension was hydrolyzed by 0.5 N HCl at 50 °C for 15 h. After hydrolysis, samples were deproteinized with methanol, followed by centrifugation at 15,000 × *g* for 5 min at 4 °C. The supernatant was then neutralized with ammonium buffer, and evaporated to dryness under reduced pressure (Savant SpeedVac concentrator, Thermo Fisher Scientific, MA, USA). The residues were resuspended in 60% methanol, and the doxorubicinone released from the polymers by acid hydrolysis was quantified by ultra-high-performance liquid chromatography by using our previously reported method (Sakai-Kato et al., 2010) to determine the amount of intracellular Dox-bound polymers (Fig. 1b). The other 50 μL of cell suspension was treated in the same way but without the hydrolysis step to evaluate the amount of free doxorubicinone, that is, doxorubicinone not derived from Dox-bound polymers. The results of three independent experiments were averaged and analyzed statistically by *t*-test.

2.4. In vitro cytotoxicity

HeLa cell lines were evaluated in the present study. The HeLa cells were maintained in monolayer cultures in DMEM containing 10% FBS and 100 U/mL penicillin/streptomycin. WST-8 Cell Counting kit-8 (Dojindo, Kumamoto, Japan) was used for cell proliferation assay. 3000 cells of HeLa cell line in 100 μL of culture medium were plated in 96 well plates and were then incubated for 24 h at 37 °C. Serial dilutions of Dox-bound polymers, micelles incorporating free Dox or just free Dox were added, and the cells were incubated for 24

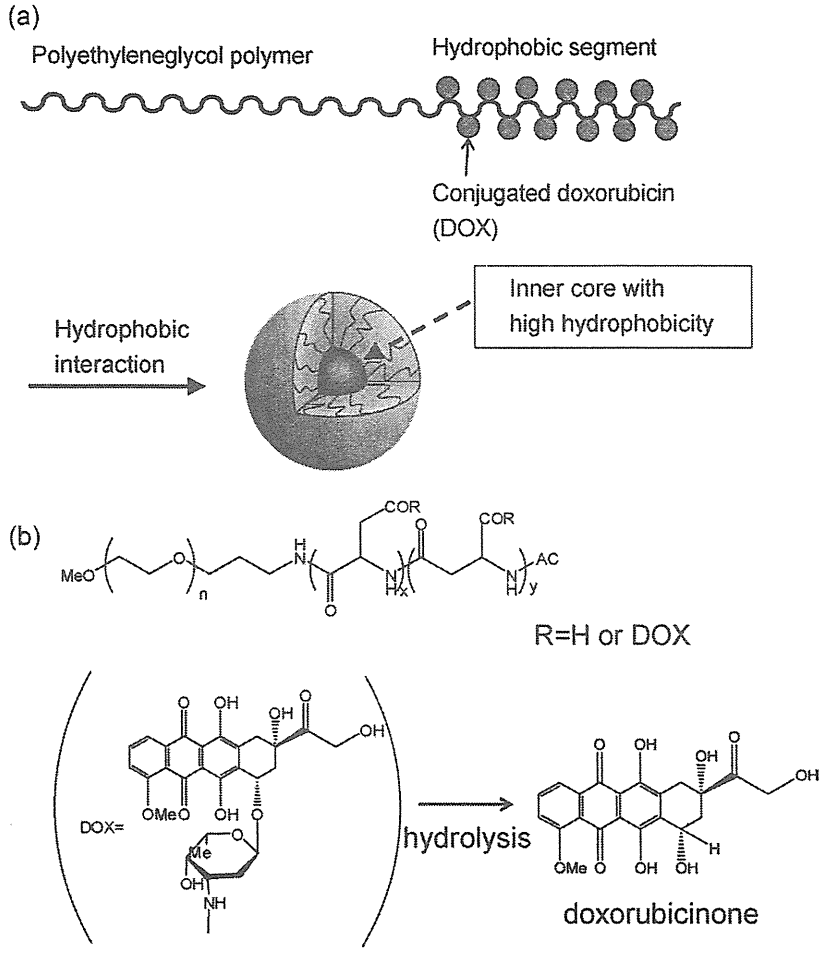

Fig. 1. Schematic of the structure of a Dox-bound polymeric micelle (a) and the chemical structure of the block copolymer (b). Polymer-bound Dox can be released as doxorubicinone by acid hydrolysis. The quantity of released doxorubicinone was used as a measure of the amount of intracellular polymers.

or 48 h. All data were expressed as mean ± SD of triplicate data. The data were then plotted as a percentage of the data from the control cultures, which were treated identically to the experimental cultures, except that no drug was added.

2.5. Confocal analysis of live cells

The intracellular trafficking of the Dox-bound micelles in live cells was examined by confocal microscopy (Carl Zeiss LSM 510, Oberkochen, Germany, or Nikon A1, Tokyo, Japan). Data were collected using dedicated software supplied by the manufacturers and exported as tagged image files (TIFs). HeLa cells (1.5×10^5) were plated in 35-mm glass-bottom dishes coated with poly-L-lysine (Matsunami) in DMEM containing 10% FBS and 100 U/mL penicillin/streptomycin. After incubation for two days (37 °C, 5% CO_2), the cells were exposed to 50 μg/mL Dox-bound polymers in culture medium. After the indicated durations, the cells were washed and kept in PBS or HBSS (Invitrogen) for imaging with the confocal microscope.

2.6. Labeling specific organelles in live cells

After incubation with Dox-bound polymers for 24 h, HeLa cells were washed with HBSS and labeled with organelle-specific fluorescent probes in accordance with the manufacturer's instructions. LysoTracker probe (Invitrogen) was used for labeling lysosomes, and ER-Tracker (Invitrogen) was used for labeling the endoplasmic reticulum (ER). A fluorescent Alexa Fluor 488 conjugate of transferrin (Alexa-transferrin; Invitrogen) was used as an exogenously added endocytic marker to delineate the endocytic recycling pathway for live cell imaging.

We also used an expression construct containing enhanced cyan fluorescent protein (ECFP) fused to an Golgi-targeting sequence derived from human β-1,4-galactosyltransferase as an Golgi localization marker (ECFP-Golgi). The construct was purchased from Clontech (Takara Bio Inc., Shiga, Japan). Cells were grown in 35-mm glass-bottom dishes coated with poly-L-lysine and transfected with Lipofectamine 2000 (Invitrogen). After overnight incubation, the cells were exposed to and allowed to internalize Dox-bound micelles for 24 h and then examined with confocal microscopy.

2.7. Efflux study of DOX-bound polymers or DBD-labeled polymers using the ABCB1 inhibitor verapamil

HeLa cells (1.5×10^5) were plated in 35-mm glass-bottom dishes coated with poly-L-lysine in DMEM containing 10% FBS and 100 U/mL penicillin/streptomycin. After incubation for two days (37 °C, 5% CO_2), the cells were exposed to 50 μg/mL Dox-bound polymers in culture medium for 3 h. Cells were washed with 50 μg/mL verapamil (Wako Pure Chemical Industries, Ltd., Osaka, Japan) (Davis et al., 2004; Kolwankar et al., 2005) or 0.1% dimethyl sulfoxide as a control. After washes, the cells were incubated for another 2 h in HBSS containing the same concentration of reagent. The cells were collected and processed for measurement of intracellular concentrations of Dox-bound polymers as described in Section 2.3. The efflux of DBD-labeled polymers was evaluated by

measurement of the fluorescent intensity inside cells using confocal microscopy. The intensity of the intracellular fluorescence was evaluated by image processing software (MetaMorph, Molecular Devices, CA, USA). The intensity of a single cell was mathematically determined by dividing the total intensity by the number of cells. Three independent experiments were averaged and analyzed statistically with the *t*-test.

2.8. Knockdown of ABCB1 by siRNA

Stealth RNAi oligonucleotides (Invitrogen) were used for siRNA experiments. Human ABCB1-siRNA sense, 5′-UCCCGUAGAAACCUUACAUUUAUGG-3′, and antisense, 5′-CCAUAAAUGUAAGGUUUCUACGGGA-3′, sequences were used. For a negative control, the Stealth RNAi Low GC Negative Control Duplex (Invitrogen) was used. The Stealth RNAi oligonucleotides were transfected into HeLa cells by using Lipofectamine RNAi MAX according to the manufacturer's protocols. After two days, the cells were exposed to 50 μg/mL Dox-bound polymers in culture medium for 3 h. After incubation, cells were washed with HBSS, and then incubated for another 2 h in HBSS without polymers. Cells were collected, and the intracellular polymers were quantified as described in Section 2.3.

2.9. Western blotting

Cells were washed with PBS and lysed in lysis buffer (20 mM Tris-HCl, pH 7.5; 1 mM EDTA; 10% glycerol; and 1% Triton X-100) containing protease inhibitors, namely, 2 mM phenylmethylsulfonyl fluoride and protease inhibitor cocktail (Sigma-Aldrich, St. Louis, MO, USA). Samples were electrophoresed on a sodium dodecyl sulfate (SDS)-polyacrylamide gel (5–20%) and transferred to a Polyvinylidene fluoride (PVDF) membrane. The blots were probed with anti-MDR (G-1) antibody (Santa Cruz Biotechnology, Inc., Santa Cruz, CA, USA) and developed with anti-mouse IgG peroxidase-linked species-specific whole antibody (from sheep) (GE Healthcare UK Limited, Little Chalfont, UK) by chemiluminescence.

3. Results and discussion

3.1. Physicochemical properties of Dox-bound micelles

The micelle carrier (Fig. 1) consisted of a block copolymer of PEG (molecular weight about 5000) and poly(aspartic acid) (polymerization degree, 30). To increase the hydrophobicity of the inner core, Dox was partially conjugated (about 45%) to the side chain of the aspartic acid. Because particle size affects the intracellular uptake of nanoparticulate formulations, we first examined the particle size of the micelles without free Dox. The Dox-bound micelles had a hydrodynamic diameter of about 42 nm at the dosed concentration of 50 μg/mL (Fig. 2a). AFM measurement of the micelles also confirmed that they were spherical with a particle size of around 40 nm (Fig. 2b). This size of micelle without free Dox is very similar to that of the micelles containing free Dox in the inner core that interacts with the conjugated Dox (Nakanishi et al., 2001), indicating that the presence of incorporated free Dox does not change the average diameter much.

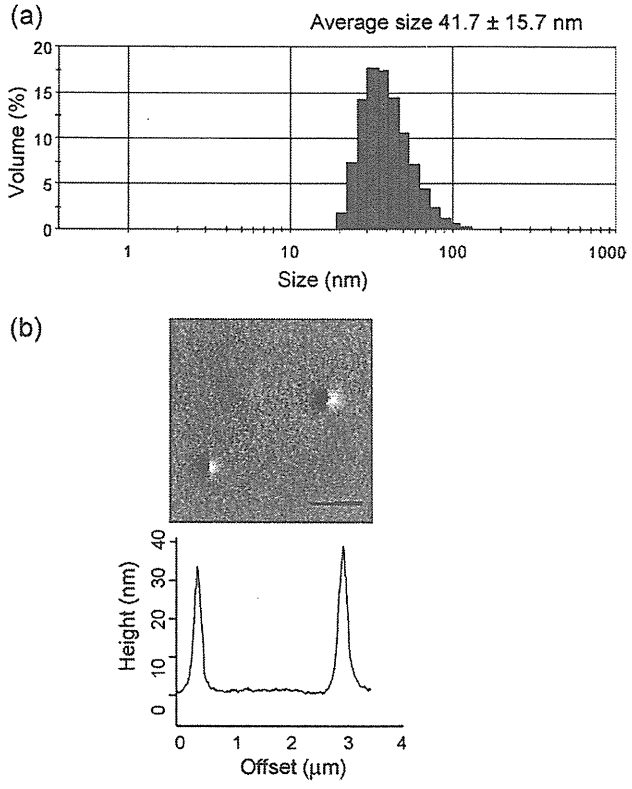

Fig. 2. Physicochemical properties of Dox-bound polymeric micelles. (a) Average size distribution of Dox-bound polymeric micelles by DLS. (b) The upper image shows an AFM image of Dox-bound polymeric micelles (bar: 1 μm) and the lower shows the cross-sectional topological profile of the image drawn in the upper panel.

3.2. In vitro cytotoxicity

We examined the *in vitro* cytotoxicity of the Dox-bound copolymers and the micelles incorporating free doxorubicin. As shown in Table 1, the cytotoxicity of doxorubicin-bound copolymers was negligible. This fact has been also reported in the previously published paper (Nakanishi et al., 2001). On the other hand, micelles incorporating free doxorubicin showed equivalent *in vitro* cytotoxic activity to free doxorubicin which is not incorporated into micelle. Therefore, in this system, the doxorubicin was conjugated to the block copolymer to increase the hydrophobicity of the inner core of the micelle so that efficient amount of free doxorubicin can be incorporated into the inner core of the micelles, and its cytotoxicity was negligible.

3.3. Intracellular uptake of Dox-bound polymers

To evaluate the intracellular uptake of Dox-bound polymers, we measured their intracellular amount by quantitating the doxorubicinone released from the intracellular polymers by acid hydrolysis treatment (Fig. 1b). Although the Dox-bound polymers contained 0.02% (w/w) free doxorubicinone as an impurity, no inherent free doxorubicinone was detected in the cells in any of the experiments in which we measured the intracellular concentration of doxorubicinone without acid hydrolysis. This result also indicates that

Table 1
IC50 values (μg/mL).

24 h			48 h		
Dox-bound polymer	Micelle incorporating free Dox	Free Dox	Dox-bound polymer	Micelle incorporating free Dox	Free Dox
>10	0.37	0.27	>10	0.045	0.024

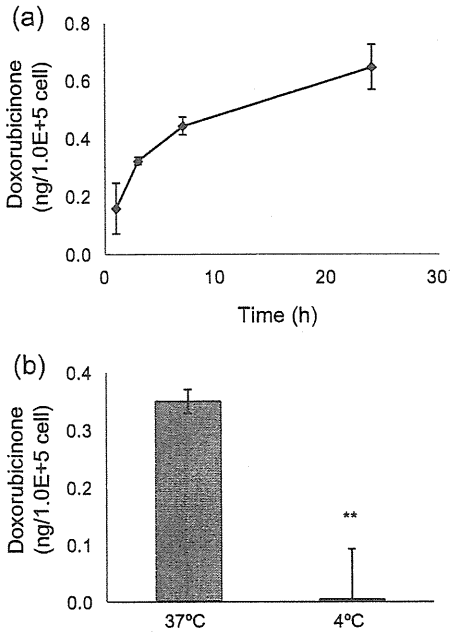

Fig. 3. Internalization of Dox-bound polymers. (a) Change in the internalized amount of Dox-bound polymers in cells as indicated by released doxorubicinone over time. HeLa cells were incubated in medium containing Dox-bound polymers for the indicated durations, followed by washes with PBS. The doxorubicinone released by acid hydrolysis was quantitated as a measure of the amount of intracellular polymers, as described in Section 2. (b) Effect of temperature on the internalization of Dox-bound polymers. HeLa cells were incubated in medium containing Dox-bound polymers at 37 °C or 4 °C for 3 h, followed by washes with PBS. The amount of intracellular polymers was quantitated by measuring the doxorubicinone released by acid hydrolysis, as described in Section 2. $^{**}P < 0.01$.

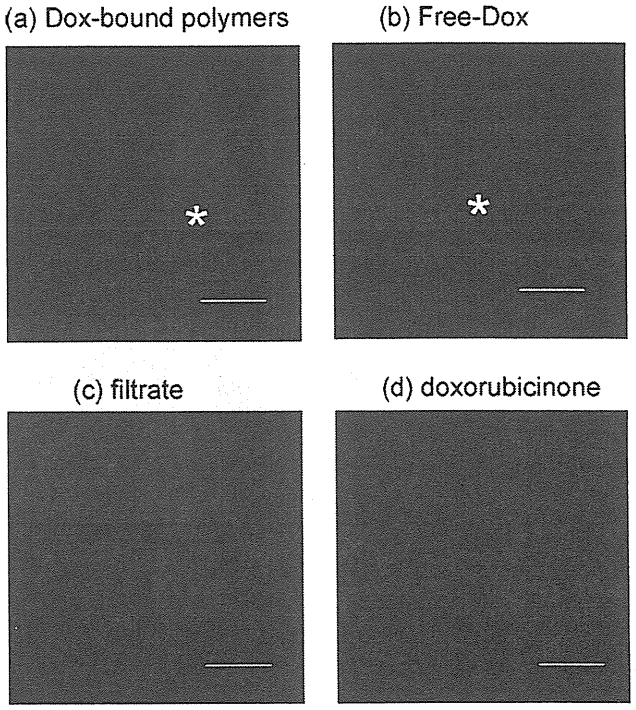

Fig. 4. Intracellular distribution of (a) DOX-bound polymers in HeLa cells exposed to 50 μg/mL Dox-bound polymers and (b) free DOX in cells exposed to 5 μg/mL free Dox for 1 h. Intracellular distribution of DOX-bound polymers in HeLa cells (c) cultured for 24 h in medium containing the filtrate of medium that was preincubated with Dox-bound polymers, and (d) cultured with 20 ng/mL free doxorubicinone for 24 h. Bars: 10 μm. Asterisk indicates the nucleus.

degradation of Dox-bound polymers that releases doxorubicinone during the experiments was negligible.

We then incubated HeLa cells in medium containing Dox-bound polymers for 1–24 h. After the incubation, the cells were washed. By determining the amounts of doxorubicinone released from Dox-bound polymers by acid hydrolysis of the cells, we were able to observe a time-dependent increase in the intracellular amount of Dox-bound polymers (Fig. 3a). Moreover, the amount of polymers in cells was significantly lower in cells incubated with the polymers at 4 °C than at 37 °C (Fig. 3b), indicating that the cells took up the polymers by endocytosis.

3.4. Intracellular distribution of Dox-bound polymers

The intracellular distribution of Dox-bound polymers was studied by confocal microscopy using the inherent fluorescence of the Dox covalently bound to the block copolymers. The Dox-bound polymers were localized in the perinuclear regions but not in the nucleus (Fig. 4a). This was different from the localization of free Dox which was distributed in the nucleus after 1 h (Fig. 4b), as reported previously (Beyer et al., 2001). This distribution will explain the fact that *in vitro* cytotoxicity of Dox-bound polymers was negligible (Table 1). To confirm that the Dox was not released from block copolymers as doxorubicinone (Fig. 1b) during the incubation time of the experiment, Dox-bound polymers were incubated in cell culture medium for 1 h at 37 °C, and then removed by centrifugal filtration using a Microcon YM-3 tube (Millipore, MA, USA). The resultant filtrate was added to the cell culture medium. Confocal microscopy showed no fluorescence within the cells (Fig. 4c). Furthermore, when HeLa cells were cultured in cell culture medium containing 20 ng/mL free doxorubicinone, which corresponds to 0.02% (w/w) of Dox-bound polymers, for 24 h, fluorescence was negligible within the cells (Fig. 4d). These results show that the fluorescence seen within the cells after Dox-bound polymer incubation is caused by the uptake of polymers and not by free doxorubicinone or Dox.

We next examined the intracellular localization of Dox-bound polymers by colocalization studies using fluorescent organelle markers. The fluorescence derived from Dox-bound polymers coincided well with the specific staining of the ER by ER-Tracker in double-labeling experiments (Fig. 5a). High-resolution images showed that both staining procedures clearly stained membranal structures (Fig. 5b).

Because the Golgi apparatus is also located in the perinuclear area and is involved in the intracellular transport of various molecules, we investigated the localization of the polymers by transfecting cells with an expression construct containing ECFP fused to a Golgi-specific protein. As shown in Fig. 5c, the distribution of polymers in the Golgi was negligible. We also confirmed that treatment of cells with Lipofectamine treatment did not affect the distribution of polymers (data not shown).

To what, then, can this particularly strong staining of the perinuclear areas be attributed? The perinuclear area is known to be the microtubule-organizing center (MTOC), an area in eukaryotic cells from which microtubules emerge and where endosomes and other endocytotic vesicles cluster (Matteoni and Kreis, 1987). In fact, a fluorescent staining image showed that the vesicles containing Dox-bound polymers in the perinuclear area (Fig. 6a, yellow arrows) coincided with the MTOC, as marked by Alexa-transferrin, an endocytic marker (Fig. 6a, white arrows). Some of the vesicles containing polymers were also stained by LysoTracker, a dye that specifically stains lysosomes (Fig. 6b). These results show that the polymers are internalized by endocytosis and transported to endosomal/lysosomal compartments. Duncan and colleagues, examined the localization of polymers by using Oregon Green as a fluorescent tag and found that three water-soluble polymeric carriers, *N*-(2-hydroxypropyl)methacrylamide, Dextran, and PEG, localized to late

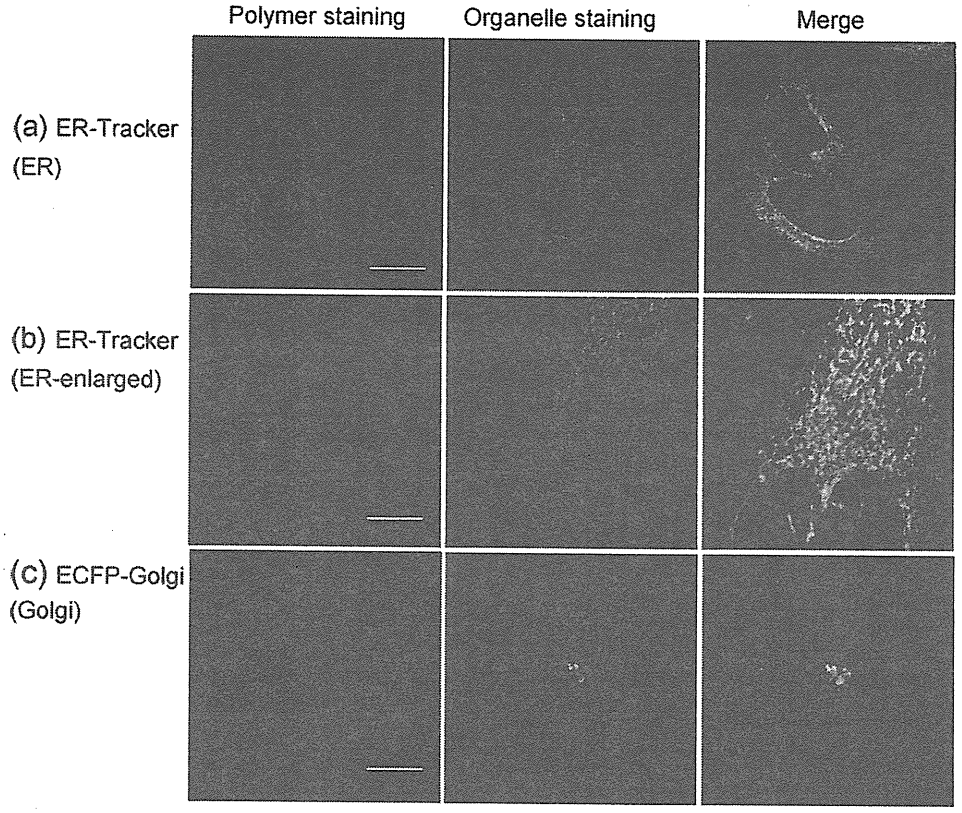

Fig. 5. Localization of Dox-bound polymers in cells co-stained with organelle-specific markers. Left, images of stained Dox-bound polymers; middle, organelle-specific fluorescent staining images; right, merged images of the left and middle images. Localization experiments using. (a and b) ER-Tracker for ER, (c) ECFP-Golgi for Golgi. Bars: 10 μm for (a) and (c). Bars: 5 μm for (b).

endosomal compartments (including lysosomes) (Richardson et al., 2008), findings consistent with our results. The perinuclear localization of the polymers is a great advantage of this system with regard to the incorporation of a nuclear-targeted drug or gene.

Most nanomaterials have been shown to exploit more than one pathway to gain cellular entry, and the pathway exploited can determine the intracellular fate (Sahay et al., 2010a). After internalization into HeLa cells, the Dox-bound polymers might be delivered to the ER directly from endosomes; in the case of cholesterol, there is some evidence for a direct pathway from endosomes to the ER (Ioannou, 2001; Mineo and Anderson, 2001). Or the polymers might be delivered to the ER directly, bypassing the endosomes/lysosomes, as do unimers of the amphiphilic triblock copolymer of poly(ethylene oxide), poly(propylene oxide), and Pluronic P85 (Sahay et al., 2010b). Simian virus 40 is known to enter the cytosol *via* the ER, suggesting that polymers distributed

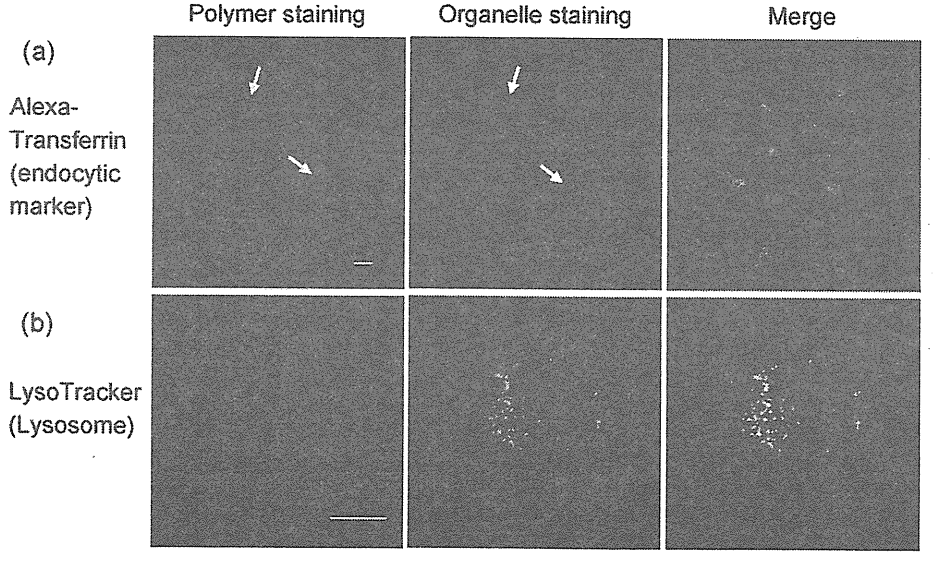

Fig. 6. Fluorescent staining images of Dox-bound polymers in cells co-stained with organelle-specific markers. Left, images of stained Dox-bound polymers; middle, organelle-specific fluorescent staining images; right, merged images of the left and middle images. Localization experiments using. (a) Alexa-transferrin, an endocytic compartment marker, and (b) LysoTracker, which is specific for lysosomes. Bars: 10 μm. Yellow and white arrows in (a) indicate the MTOC area.

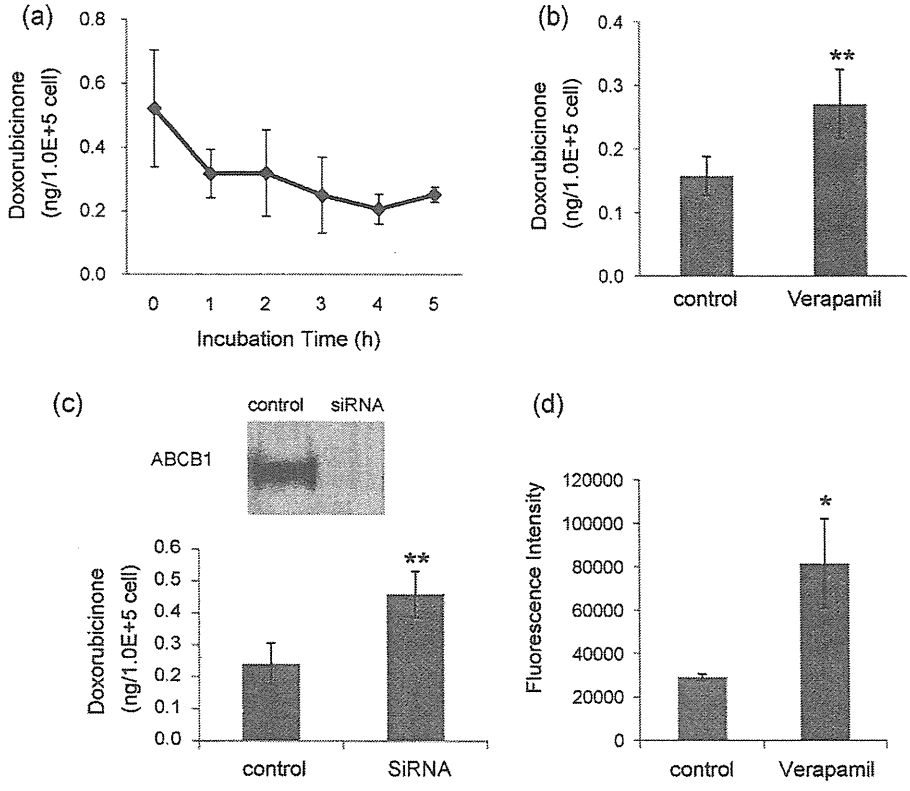

Fig. 7. Efflux of Dox-bound polymers. (a) Time-dependent change in intracellular Dox-bound polymers as indicated by released doxorubicinone. After incubation in medium with Dox-bound polymers, HeLa cells were washed and incubated with HBSS at 37 °C for the indicated durations. The doxorubicinone released by acid hydrolysis was quantitated as the amount of intracellular polymers as described in Section 2. (b) Effect of ABCB1 transporter on the efflux of Dox-bound polymers. HeLa cells were exposed to 50 μg/mL Dox-bound polymers in culture medium for 3 h. Cells were washed with 50 μg/mL verapamil or 0.1% dimethyl sulfoxide as a control. Then, the cells were incubated for another 2 h in HBSS containing the same concentration of each reagent. The amount of intracellular polymers was quantitated as the amount of doxorubicinone released by acid hydrolysis, as described in Section 2. $^{**}P < 0.01$. (c) Effect of the knockdown of ABCB1 transporter expression by siRNA on the efflux of Dox-bound polymers. Expression of ABCB1 in cell extracts was analyzed by immunoblot analysis (top). After 2 days of siRNA transfection, the cells were exposed to 50 μg/mL of Dox-bound polymers in culture medium for 3 h. After incubation, the cells were washed with HBSS and then incubated for another 2 h in HBSS without polymer. The amount of intracellular polymers was quantitated as the amount of doxorubicinone released by acid hydrolysis, as described in Section 2 (bottom). $^{**}P < 0.01$. Effect of ABCB1 transporter on the efflux of DBD-labeled polymers. HeLa cells were exposed to 50 μg/mL DBD-labeled polymers in culture medium for 24 h. Cells were washed with 50 μg/mL verapamil or 0.1% dimethyl sulfoxide as a control. Then, the cells were incubated for another 2 h in HBSS containing the same concentration of each reagent. The fluorescence intensity in a single cell was calculated as described in Section 2. $^{*}P < 0.05$.

in the ER might similarly gain access to the cytosol (Damm et al., 2005). The characteristic distribution pattern of the polymers did not change much with increasing incubation times from 0.5 to 24 h (data not shown). Although it is not clear whether the polymers maintain their structure as globular micelles or exist as unimers after internalization into a cell, increasing the dosed polymer concentration to 1 mg/mL did not change the staining pattern (data not shown). Recently, we showed PEG and poly(glutamic acid) block copolymer micelles incorporating dichloro(1,2-diaminocyclohexane)platinum(II) selectively dissociate within late endosomes (Murakami et al., 2011), suggesting that the Dox-bound polymers might also dissociate.

3.5. *Efflux of Dox-bound polymers from HeLa cells to medium*

As described in Section 3.2, the amount of intracellular Dox-bound polymers increased with time when cells were continuously exposed to Dox-bound polymers (Fig. 3a). In contrast, the amount of Dox-bound polymers gradually decreased after the Dox-bound polymers were removed from the medium (Fig. 7a). Interestingly, this decrease in the intracellular amount of Dox-bound polymers was abolished in the presence of verapamil, an inhibitor of ABCB1 (ATP-binding cassette protein B1) transporter (Fig. 7b). The ABCB1 transporter, which is also known as multidrug resistance 1 (MDR-1) or P-glycoprotein, is a member of the ABC-type transporter family and an efflux pump for various drugs. To further investigate the role of this transporter in the efflux of Dox-bound polymers from cells to medium, small interference RNAs (siRNAs) were used to target ABCB1 RNA in HeLa cells. Two days after transfection of synthetic siRNA, Western blot analysis showed that levels of ABCB1 protein expression in siRNA-transfected HeLa cells were drastically decreased (Fig. 7c), and the efflux of Dox-bound polymers from these cells was also significantly inhibited (Fig. 7c). The efflux of DBD-labeled polymers was also inhibited by ABCB1 transporter inhibitor, when intracellular fluorescent intensity of DBD-labeled polymers was measured (Fig. 7d). These results suggest that ABCB1 transporter is a key regulator of the clearance of Dox-bound polymers from HeLa cells.

It is reported that drug-binding site of ABCB1 transporter is located at a drug binding pocket that is formed by transmembrane segments and allow access of molecules directly from the membranes (Aller et al., 2009; Loo et al., 2003a,b). Furthermore, it is also known that subdomains of the ER form close contact with plasma membrane and some proteins may regulate the formation of direct membrane contacts that facilitate sterol exchange between the ER and plasma membrane (Ikonen, 2008).

Therefore, it is probable that a part of Dox-bound polymers localized in ER are transported to plasma membrane and then recognized at the drug binding site in the transmembrane segments of ABCB1 transporter.

In general, the ABCB1 transporter has very broad substrate specificity: recent studies have shown that it mediates the efflux

of a relatively large peptide, amyloid β peptide (molecular weight, 4.5 kDa), across the blood–brain barrier into the bloodstream (Cirrito et al., 2005; Kuhnke et al., 2007; Lam et al., 2001). To the best of our knowledge, the ABCB1 transporter has not been reported before to be involved in the clearance of block copolymers from cells. Because ABCB1 transporter is expressed primarily in certain normal cell types in the liver, kidney, and jejunum (Thiebaut et al., 1987), the role of ABCB1 transporter as excretion pump of Dox-bound polymer and the effect of ABCB1 transporter on the polymer blood level are probably significant from a safety perspective.

Taken together, the findings presented here suggest that Dox-bound polymers are incorporated by endocytosis. Some of the incorporated polymers are transferred to the endosome/lysosome system, and the rest may bypass the endosomal system. Then, the polymers are likely delivered to other compartments, including ER and the plasma membrane. The excretion of excess polymers from the cells is mediated by the ABCB1 transporter. Although in this system, the conjugated Dox was not designed to be released from the polymers, our results concerning intracellular trafficking and clearance of polymers would be very useful to design the carrier system where bound drugs are released from the carrier for pharmacological activity.

4. Conclusion

We investigated the intracellular trafficking of Dox-bound polymers. The polymers are internalized into cells by endocytosis, then transported to endosomal/lysosomal compartments, followed by partial distribution to the ER, or transported directly to the ER. The active excretion of the polymers from the cells may be mediated by the ABCB1 transporter. It is surprising that cells utilize their endogenous transport system for intracellular trafficking of this artificial drug carrier. Our results potentially can contribute not only to the discussion of safety issues of polymeric therapeutics but also the development of a DDS strategy utilizing or targeting this endogenous pathway more effectively.

Acknowledgements

The authors are grateful for support from Research on Publicly Essential Drugs and Medical Devices (Japan Health Sciences Foundation), a Health Labor Sciences Research Grant, and the Global COE Program for the Center for Medical System Innovation, MEXT, KAKENHI (21790046), and Nippon Kayaku Co. Ltd. We thank Mr. R. Nakamura (Nikon Corp.) for technical assistance.

References

Allen, C., Maysinger, D., Eisenberg, A., 1999. Nano-engineering block copolymer aggregates for drug delivery. Colloids Surf. B: Biointerfaces 16, 3–27.

Aller, S.G., Yu, J., Ward, A., Weng, Y., Chittaboina, S., Zhuo, R., Harrell, P.M., Trinh, Y.T., Zhang, Q., Urbatsch, I.L., Chang, G., 2009. Structure of P-glycoprotein reveals a molecular basis for poly-specific drug binding. Science 323, 1718–1722.

Bae, Y., Kataoka, K., 2009. Intelligent polymeric micelles from functional poly (ethylene glycol)-poly (amino acid) block copolymers. Adv. Drug Deliv. Rev. 61, 768–784.

Beyer, U., Rothern-Rutishauser, B., Unger, C., Wunderli-Allenspach, H., Kratz, F., 2001. Differences in the intracellular distribution of acid-sensitive doxorubicin-protein conjugates in comparison to free and liposomal formulated doxorubicin as shown by confocal microscopy. Pharm. Res. 18, 29–38.

Cirrito, J.R., Deane, R., Fagan, A.M., Spinner, M.L., Parsadanian, M., Finn, M.B., Jiang, H., Prior, J.L., Sagare, A., Bales, K.R., Paul, S.M., Zlokovic, B.V., Piwnica-Worms, D., Holtzman, D.M., 2005. P-glycoprotein deficiency at the blood-brain barrier increases amyloid-beta deposition in an Alzheimer disease mouse model. J Clin. Invest. 115, 3285–3290.

Damm, E.M., Pelkmans, L., Kartenbeck, J., Mezzacasa, A., Kurzchalia, T., Helenius, A., 2005. Clathrin- and caveolin-1-independent endocytosis: entry of simian virus 40 into cells devoid of caveolae. J. Cell Biol. 168, 477–488.

Davis, B.M., Humeau, L., Slepushkin, V., Binder, G., Korshalla, L., Ni, Y., Ogunjimi, E.O., Chang, L.F., Lu, X., Dropulic, B., 2004. ABC transporter inhibitors that are substrates enhance lentiviral vector transduction into primitive hematopoietic progenitor cells. Blood 104, 364–373.

Ferrari, M., 2005. Cancer nanotechnology: opportunities and challenges. Nat. Rev. Cancer 5, 161–171.

Hamaguchi, T., Kato, K., Yasui, H., Morizane, C., Ikeda, M., Ueno, H., Muro, K., Yamada, Y., Okusaka, T., Shirao, K., Shimada, Y., Nakahama, H., Matsumura, Y., 2007. A phase I and pharmacokinetic study of NK105, a paclitaxel-incorporating micellar nanoparticle formulation. Br. J. Cancer 97, 170–176.

Hopkins, A.L., Groom, C.R., 2002. The druggable genome. Nat. Rev. Drug Discov. 1, 727–730.

Hughes, B., 2009. Gearing up for follow-on biologics. Nat. Rev. Drug Discov. 8, 181.

Ikonen, E., 2008. Cellular cholesterol trafficking and compartmentalization. Nat. Rev. Mol. Cell Biol. 9, 125–138.

Illum, L., Davis, S.S., Müller, R.H., Mak, E., West, P., 1987. The organ distribution and circulation time of intravenously injected colloidal carriers sterically stabilized with a blockcopolymer-poloxamine 908. Life Sci. 40, 367–374.

Ioannou, Y.A., 2001. Multidrug permeases and subcellular cholesterol transport. Nat. Rev. Mol. Cell Biol. 2, 657–668.

Kataoka, K., Kwon, G.S., Yokoyama, M., Okano, T., Sakurai, Y., 1993. Block copolymer micelles as vehicles for drug delivery. J. Control. Rel. 24, 119–132.

Kataoka, K., Harada, A., Nagasaki, Y., 2001. Block copolymer micelles for drug delivery: design, characterization and biological significance. Adv. Drug Deliv. Rev. 47, 113–131.

Kolwankar, D., Glover, D.D., Ware, J.A., Tracy, T.S., 2005. Expression and function of ABCB1 and ABCG2 in human placental tissue. Drug Metab. Dispos. 33, 524–529.

Kuhnke, D., Jedlitschky, G., Grube, M., Krohn, M., Jucker, M., Mosyagin, I., Cascorbi, I., Walker, L.C., Kroemer, H.K., Warzok, R.W., Vogelgesang, S., 2007. MDR1-P-glycoprotein (ABCB1) mediates transport of Alzheimer's amyloid-β peptides – implications for the mechanisms of Aβ clearance at the blood–brain barrier. Brain Pathol. 17, 347–353.

Kuroda, J., Kuratsu, J., Yasunaga, M., Koga, Y., Saito, Y., Matsumura, Y., 2009. Potent antitumor effect of SN-38-incorporating polymeric micelle, NK012, against malignant glioma. Int. J. Cancer 124, 2505–2511.

Lam, F.C., Liu, R., Lu, P., Shapiro, A.B., Renoir, J.-M., Sharom, F.J., Reiner, P.B., 2001. β-Amyloid efflux mediated by p-glycoprotein. J. Neurochem. 76, 1121–1128.

Lavasanifar, A., Samuel, J., Kwon, G.S., 2002. Poly(ethylene oxide)-block-poly (L-amino acid) micelles for drug delivery. Adv. Drug Deliv. Rev. 54, 169–190.

Lee, S.M., Kim, J.S., 2005. Intracellular trafficking of transferrin-conjugated liposome/DNA complexes by confocal microscopy. Arch. Pharm. Res. 28, 93–99.

Lipinski, C.A., Lombardo, F., Dominy, B.W., Feeney, P.J., 2001. Experimental and computational approaches to estimate solubility and permeability in drug discovery and development settings. Adv. Drug Deliv. Rev. 46, 3–26.

Loo, T.W., Bartlett, M.C., Clarke, D.M., 2003a. Substrate-induced conformational changes in the transmembrane segments of human P-glycoprotein. J. Biol. Chem. 278, 13603–13606.

Loo, T.W., Bartlett, M.C., Clarke, D.M., 2003b. Methanethiosulfonate derivatives of rhodamine and verapamil activate human P-glycoprotein at different sites. J. Biol. Chem. 278, 50136–50141.

Manunta, M., Izzo, L., Duncan, R., Jones, A.T., 2007. Establishment of subcellular fractionation techniques to monitor the intracellular fate of polymer therapeutics. II. Identification of endosomal and lysosomal compartments in HepG2 cells combining single-step subcellular fractionation with fluorescent imaging. J. Drug Target. 15, 37–50.

Matsumura, Y., Maeda, H., 1986. A new concept for macromolecular therapeutics in cancer chemotherapy: mechanism of tumoritropic accumulation of proteins and the antitumor agent smancs. Cancer Res. 46, 6387–6392.

Matsumura, Y., Hamaguchi, T., Ura, T., Muro, K., Yamada, Y., Shimada, Y., Shirao, K., Okusaka, T., Ueno, H., Ikeda, M., Watanabe, N., 2004. Phase I clinical trial and pharmacokinetic evaluation of NK911, a micelle-encapsulated doxorubicin. Br. J. Cancer 91, 1775–1781.

Matteoni, R., Kreis, T.E., 1987. Translocation and clustering of endosomes and lysosomes depends on microtubules. J. Cell Biol. 105, 1253–1265.

Mineo, C., Anderson, R.G., 2001. Potocytosis. Robert Feulgen lecture. Histochem. Cell Biol. 116, 109–118.

Murakami, M., Cabral, H., Matsumoto, Y., Wu, S., Kano, M.R., Yamori, T., Nishiyama, N., Kataoka, K., 2011. Improving drug potency and efficacy by nanocarrier-mediated subcellular targeting. Sci. Transl. Med. 3, 64ra2.

Nakanishi, T., Fukushima, S., Okamoto, K., Suzuki, M., Matsumura, Y., Yokoyama, M., Okano, T., Sakurai, Y., Kataoka, K., 2001. Development of the polymer micelle carrier system for doxorubicin. J. Control. Rel. 74, 295–302.

Nishiyama, N., Kataoka, K., 2006. Current state, achievements, and future prospects of polymeric micelles as nanocarriers for drug and gene delivery. Pharmacol. Ther. 112, 630–648.

O'Brien, M.E.R., Wigler, N., Inbar, M., Rosso, R., Grischke, E., Santoro, A., Catane, R., Kieback, D.G., Tomczak, P., Ackland, S.P., Orlandi, F., Mellars, L., Alland, L., Tendler, C., 2004. Reduced cardiotoxicity and comparable efficacy in a phase III trial of pegylated liposomal doxorubicin HCl (CAELYX™/Doxil®) versus conventional doxorubicin for first-line treatment of metastatic breast cancer. Ann. Oncol. 15, 440–449.

Olson, R.D., Mushlin, P.S., Brenner, D.E., Fleischer, S., Cusack, B.J., Chang, B.K., Boucek Jr., R.J., 1988. Doxorubicin cardiotoxicity may be caused by its metabolite, doxorubicinol. Proc. Natl. Acad. Sci. U.S.A. 85, 3585–3589.

Rejman, J., Bragonzi, A., Conese, M., 2005. Role of clathrin- and caveolae-mediated endocytosis in gene transfer mediated by lipo- and polyplexes. Mol. Ther. 12, 468–474.

Richardson, S.C., Wallom, K.L., Ferguson, E.L., Deacon, S.P., Davies, M.W., Powell, A.J., Piper, R.C., Duncan, R., 2008. The use of fluorescence microscopy to define polymer localisation to the late endocytic compartments in cells that are targets for drug delivery. J. Control. Rel. 127, 1–11.

Sahay, G., Batrakova, E.V., Kabanov, A.V., 2008. Different internalization pathways of polymeric micelles and unimers and their effects on vesicular transport. Bioconjug. Chem. 19, 2023–2029.

Sahay, G., Alakhova, D.Y., Kabanov, A.V., 2010a. Endocytosis of nanomedicines. J. Control. Rel. 145, 182–195.

Sahay, G., Gautam, V., Luxenhofer, R., Kabanov, A.V., 2010b. The utilization of pathogen-like cellular trafficking by single chain block copolymer. Biomaterials 31, 1757–1764.

Sakai-Kato, K., Saito, E., Ishikura, K., Kawanishi, T., 2010. Analysis of intracellular doxorubicin and its metabolites by ultra-high-performance liquid chromatography. J. Chromatogr. B 878, 1466–1470.

Savić, R., Luo, L., Eisenberg, A., Maysinger, D., 2003. Micellar nanocontainers distribute to defined cytoplasmic organelles. Science 300, 615–618.

Thiebaut, F., Tsuruo, T., Hamada, H., Gottesman, M.M., Pastan, I., Willingham, M.C., 1987. Cellular localization of the multidrug-resistance gene product P-glycoprotein in normal human tissues. Proc. Natl. Acad. Sci. U.S.A. 84, 7735–7738.

Torchilin, V.P., 2002. PEG-based micelles as carriers of contrast agents for different imaging modalities. Adv. Drug Deliv. Rev. 54, 235–252.

Torchilin, V.P., Lukyanov, A.N., Gao, Z., Papahadjopoulos-Sternberg, B., 2003. Immunomicelles: targeted pharmaceutical carriers for poorly soluble drugs. Proc. Natl. Acad. Sci. U.S.A. 100, 6039–6044.

Yokoyama, M., Okano, T., Sakurai, Y., Fukushima, S., Okamoto, K., Kataoka, K., 1999. Selective delivery of adriamycin to a solid tumor using a polymeric micelle carrier system. J. Drug Target. 7, 171–186.

A New Approach to Characterization of Insulin Derived from Different Species Using ^{1}H-NMR Coupled with Multivariate Analysis

Akiko Ohno,*[,a] Toru Kawanishi,[b] Haruhiro Okuda,[a] and Kiyoshi Fukuhara[a]

[a] *Division of Organic Chemistry, National Institute of Health Sciences: and* [b] *Division of Drugs, National Institute of Health Sciences; Setagaya-ku, Tokyo 158–8501, Japan.*

Received October 7, 2011; accepted December 8, 2011; published online December 27, 2011

Most of the active components of polypeptides have a complex molecular structure, large molecular size. Such components may also be structurally heterogeneous. Therefore, development of a method that can confirm the consistency of polypeptides amino-acid sequences for product characterization is desirable. In general, it is extremely difficult to distinguish differences of a few amino acid residues in the ^{1}H-NMR spectrum of polypeptides with molecular weights greater than several thousand. However, we have been able to distinguish between three insulin species differing in one to three amino acid residues using a combination of multivariate statistics and ^{1}H-NMR spectra. These results demonstrate that this methodology could be useful for characterization of polypeptides.

Key words insulin; polypeptide; characterization; principal component analysis; ^{1}H-NMR

Nuclear magnetic resonance (NMR), which is frequently used for structure identification of unknown chemical substances in the fields of organic and natural products chemistry, is the only technique that can provide structural information on all of the components of a chemical substances. Although NMR techniques uniquely provide spectral information on primary and higher-order structure of large polymeric compounds such as polypeptides, such spectra are generally difficult to analyze in detail because of their complexity. NMR measurement has usually been applied to the structural analysis of single chemical substances, and to date, been not suitable for analyzing samples that contain multiple compounds because of the problem of overlapping peaks in the ^{1}H-NMR spectrum. However, NMR techniques have come to be used recently to analyze biogenic substances, which have made it possible to discriminate between small spectral differences by performing statistical analysis of the ^{1}H-NMR spectral data. Multivariate statistical methods, such as principal component analysis (PCA) and partial least-squares discriminate analysis (PLS-DA), are often useful for profiling and classifying sample groups and for characterizing the most effective variables of separated compounds.[1,2] Currently, multivariate statistical methods, which combine various analytical methods, have been widely used to evaluate the quality of drugs and foods, quantitatively or qualitatively, in addition to enabling predictions of drug metabolism, and toxicity.[3—10]

Compared with small-molecule drugs, polypeptides are heterogeneous and are more complex in their makeup for a number of possible reasons including mutations in the amino acid sequence of the protein, different posttranslational modifications, or by being a mixture of molecules with different terminal structures due to degradation by contaminating proteases.[11] The structural heterogeneity caused by these factors may affect the physiological activity and pharmacokinetics of polypeptides, resulting in changes in drug efficacy and safety.[11] Therefore, the development of analytical procedures that can confirm the constancy of multiple amino-acid sequences of a polypeptide for product characterization is desirable. However, characterizing the full complexity of polypeptides by presently available analytical methods is still difficult. Therefore, it is necessary to provide a more detailed evaluation of special characteristics of polypeptides by a new physicochemical index or new analytical techniques. In our recent study, it was reported that peak changes in the determination of characteristic spectral changes associated with time-dependent alterations of oxytocin (OXT) were also observed in the PCA loading plot.[8,12] Thus, the possibility of evaluating slight differences in the quality of a polypeptide was demonstrated.

In this study, we examined multivariate statistics coupled with ^{1}H-NMR to analyze the difference of amino acid sequences in three species of insulin and to show this method to be effective for the characterization of the polypeptides. As a result, we have succeeded in precisely characterizing human, bovine, and porcine insulins with sequence differences of one or three amino acids, by performing ^{1}H-NMR measurements of the individual insulins and their mixtures followed by PCA of the spectra. The results suggest that this methodology could be useful for the characterization of species-related sequence differences in polypeptides.

Experimental

Chemicals and Reagents All reagents used for ^{1}H-NMR experiments were of analytical grade (purity >99%) from Wako Chemicals and were used without further purification. Human recombinant insulin expressed in yeast (CAS# 11061-68-0) and insulin from bovine pancreas (CAS# 11070-73-8) were purchased from Aldrich (St. Louis, MO, U.S.A.); porcine insulin (CAS# 12584-58-6) was purchased from MP Biomedicals. Acetonitrile-d_3 for NMR was purchased from Acros Organics (CN). Deuterium oxide (D_2O, isotopic purity 99.9%) and 3-(trimethylsilyl) propionic-2,2,3,3-d_4 acid, sodium salt (TSP) were purchased from Aldrich (St. Louis, MO, U.S.A.). TSP was used as an internal standard with a chemical shift (δ) of 0.0 ppm in ^{1}H-NMR measurements.

Sample Preparation and ^{1}H-NMR Spectroscopic Analysis Each insulin (14.7 mg) was dissolved in 140 μL of 0.1 N HCl, 70 μL of 0.1 N NaOH, 200 μL of Milli-Q water, 70 μL of 5 mM TSP/D_2O, and the pH was adjusted to 3.6 by adding aliquots of 0.1 N NaOH or HCl. Milli-Q water was added to give a total volume of 910 μL, and this mixture solution was diluted with 490 μL of CD_3CN. The solvent used in the present work was H_2O/D_2O : CD_3CN (65/35 vol%). For ^{1}H-NMR

* To whom correspondence should be addressed. e-mail: ako-ohno@nihs.go.jp

Table 1. Each Insulin Mixture of the Sample Used in This Experiment: Human Insulin (A), Bovine Insulin (B), and Porcine Insulin (C)

Sample	A	:	B	:	C
A1	1		—		—
A4B1	4		1		—
A1B1	1		1		—
A1B4	1		4		—
B1	—		1		—
B4C1	—		4		1
B1C1	—		1		1
B1C4	—		1		4
C1	—		—		1
A1C4	1		—		4
A1C1	1		—		1
A4C1	4		—		1
A1B1C1	1		1		1
A2B1C1	2		1		1
A1B2C1	1		2		1
A1B1C2	1		1		2

measurements, a total sample volume of 700 μL with at least a 1.7 mM concentration (pH 3.6) was used.[13] Samples of each insulin mixture ratio are shown in Table 1.

The sample was introduced into an NMR test tube, and nuclear Overhauser effect spectroscopy (^{1}H-NOESY) spectra were recorded at 25°C using a Varian 600 MHz NMR spectrometer equipped with a cold probe. Thirty-two free induction decays (FIDs) with 75 K data points per FID were collected using a spectral width of 9615.4 Hz, an acquisition time of 4.00 s, and a total pulse recycle delay of 2.02 s. The water resonance was suppressed using presaturation during the first increment of the NOESY pulse sequence, with irradiation occurring during the 2.0 s relaxation delay and also during the 200 ms mixing time. Prior to Fourier transformation, the FIDs were zero-filled to 128 K and an exponential line broadening factor of 0.5 Hz was applied.[9,14] Spectral ^{1}H-NMR assignments were achieved according to the literature values of chemical shifts in various media.[13]

NMR Data Reduction and Preprocessing All ^{1}H-NMR spectra were phased and baseline corrected by Chenomx NMR Suite 6.0 software, professional edition (Chenomx Inc., Canada). ^{1}H-NMR spectra were subdivided into regions having an equal bin size of 0.04 ppm over a chemical shift range of 0.04—10.0 ppm (excluding the region around the water signal; 4.2—4.6 ppm), and the regions within each bin were integrated. The integrated intensities were then normalized to the total spectral area, and the data were converted from the Chenomx software format into Microsoft Excel format (*.xlt). The resulting data sets were then imported into SIMCA-P version 12.0 (Umetrics AB, Umeå, Sweden) for multivariate statistical analysis.

Multivariate Data Analysis PCA was performed to examine the intrinsic variation in the data sets. The quality of the models was described by the R^2x and Q^2 parameters, which indicate the proportion of variance in the data explained by the models and the goodness of fit. R^2x represents the goodness of fit of the PCA model, and Q^2 expresses the predictability of the PCA model. The quality of the PCA models was described by the total variance of principal component 1 (PC1) and principal component 2 (PC2) at a confidence level of 95%.

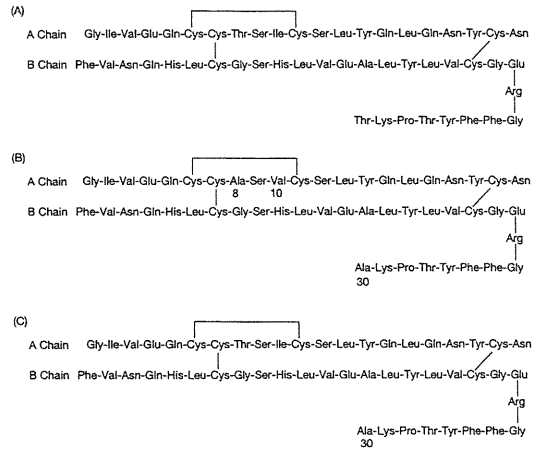

Fig. 1. Amino Acid Sequences of Human Insulin (A), Bovine Insulin (B), and Porcine Insulin (C)

Results

The amino-acid sequences of human, bovine, and porcine insulins are shown in Fig. 1. Bovine insulin differs from human insulin at the following positions: alanine (Ala) for threonine (Thr) at position A8 (8th position on the A Chain), valine (Val) for isoleucine (Ile) at A10, and Ala for Thr at the carboxyl terminus of the B-chain. Porcine insulin differs from human insulin with an Ala substituted for Thr at the carboxy terminus of the B-chain. ^{1}H-NMR spectra of the three types of insulin are shown in Fig. 2. While a simple visual inspection suggests that the three spectra might be indistinguishable, actual spectral differences may be detected if changes can be represented as points in a multidimensional space and examined using PCA. PCA of each insulin spectrum was performed, and distinct differences among the ^{1}H-NMR spectra at each sample mixture ratio were readily detected by the scores of both PC1 and PC2, which could be clearly depicted as points on the lines of the triangular phase diagram as shown in Fig. 3. In the PC1-PC2 plane, all samples were displayed in a triangular phase diagram bearing the three types of single composition insulin at each vertex. The cumulative contribution rate by PCA of the first two principal components, PC1 and PC2, was 63.8 and 83.3%, respectively. Thus, a spectrum change was characterized by PC1 and PC2 with species-related differences of insulin at a high contribution ratio. This result suggests a large contribution of human and bovine insulin to PC1, indicating that the positive direction from the center of the PC1 coordinate on the horizontal axis corresponded to bovine insulin and the negative direction corresponded to human insulin. Meanwhile, a high contribution to PC2 indicated that the positive direction from the center of the PC2 coordinate on the vertical axis corresponded to porcine insulin and the negative direction corresponded to human and bovine insulin. In addition, the mixed sample of all three types of insulin in a 1:1:1 ratio is in the center of the triangular phase diagram, and samples of each insulin mixture ratio radiate from the center toward each vertex.

The loading plot of all the evaluated ^{1}H-NMR signals is shown in Fig. 4. Each variable represents a peak at a particular chemical shift in the ^{1}H-NMR spectra shown in Fig.

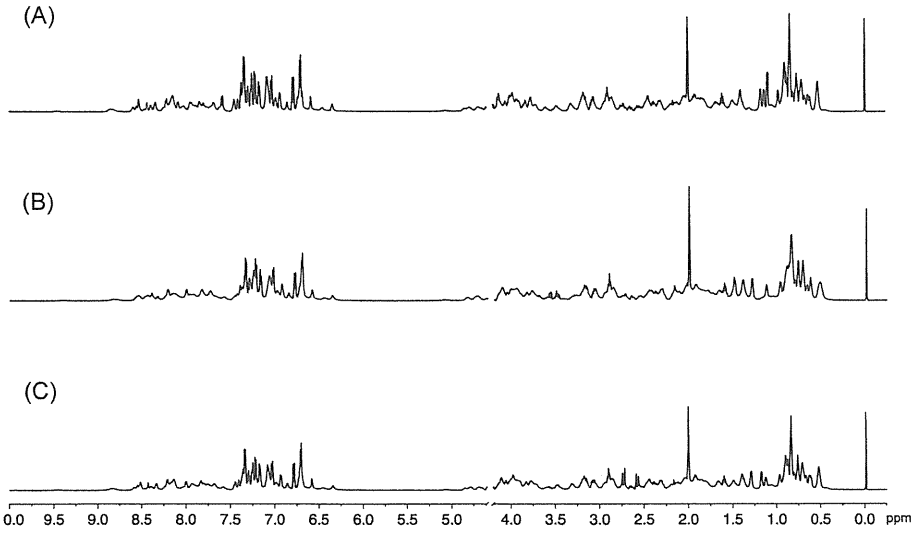

Fig. 2. ^{1}H-NMR Spectra of Human Insulin (A), Bovine Insulin (B), and Porcine Insulin (C)

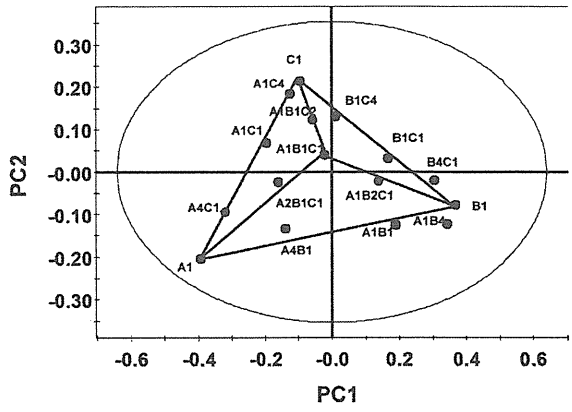

Fig. 3. PCA Scores Plot (PC1/2) Derived from the ^{1}H-NMR Spectral Data for Each Mixed Insulin Ratio

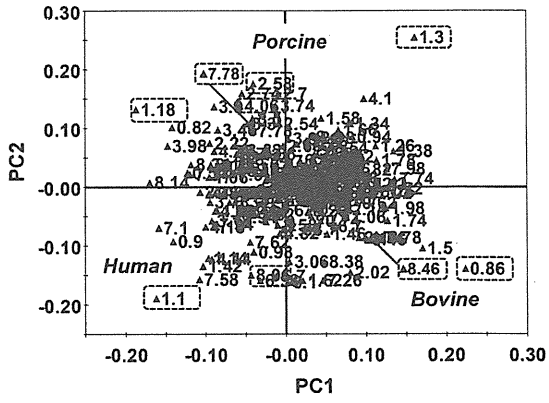

Fig. 4. The PCA Loading Plot (PC1/2) Derived from the ^{1}H-NMR Spectral Data for Each Mixed Insulin Ratio

1. This loading plot reveals the contributions of particular variables towards either an increase or decrease in the integrated intensities of the ^{1}H-NMR spectra. Six variables showing typical fluctuations of the different insulin species were identified (Fig. 4), and the integrated intensities of these variables corresponding to the insulin ratios are shown in Fig. 5. The tendency of the intensity of each of these variables to either increase or decrease is evident in the differences of the mixed insulin ratios and suggests specificity of the variables for the different insulin species. The corresponding characteristic variables of human, bovine, and porcine insulin were δ 1.1, 0.86 and 4.06 ppm, respectively. In addition, a common characteristic variable of bovine and porcine insulin occurred at δ 1.3 ppm and that of human and porcine insulin occurred at δ 1.18 ppm. The typical chemical shifts responsible for these variables were shown in Fig. 6. Therefore, these variables were indicative of the species specificity of insulin since the insulin species characterized by each variable tended to have a high intensity either for a single insulin species or for a species making up a high proportion of the mixture as shown in Fig. 5. Next, we examined whether the larger variables characterizing each species were derived from the type of amino acid residue by analysis of the loading and trend plots.

First, determination of the variables contributing significantly to the variation of the PC1 coordinate axis for the human and bovine insulin groups was performed by analysis of the amino acid residue peaks corresponding to these particular variables. Peaks for each variable could be identified: the variable at 1.1 ppm was attributed to both the γH of Ile at A10 and to the γH of Thr at B30; the variable of the amide group region at 8.06 ppm was attributed to the NH of Thr at A8 of the characteristic amino-acid sequences of human insulin. On the other hand, the variable at 0.86 ppm was attributed to the γH of Val at A10; and the variable at 1.5 ppm was attributed to the βH of Ala at A8 and/or B30; the variable of the amide group region at 8.46 ppm was attributed to the NH of Val at A10 of the characteristic amino-acid sequences of bovine insulin.

Next, determination of the variables contributing significantly to the variation of the PC2 coordinate axis for the two groups, porcine, and both human and bovine was performed by the analysis of the amino acid residue peaks corresponding to these particular variables. Peaks for each variable could be identified: the variable at 4.06 ppm was attributed to the αH of Ala at B30; the variable of the amide group region at 7.78 ppm was attributed to the NH of Ala at B30 of the characteristic amino-acid sequences of porcine insulin. Therefore, identified amino acids for each characteristic variable were by inference associated with the primary structure of the three types of

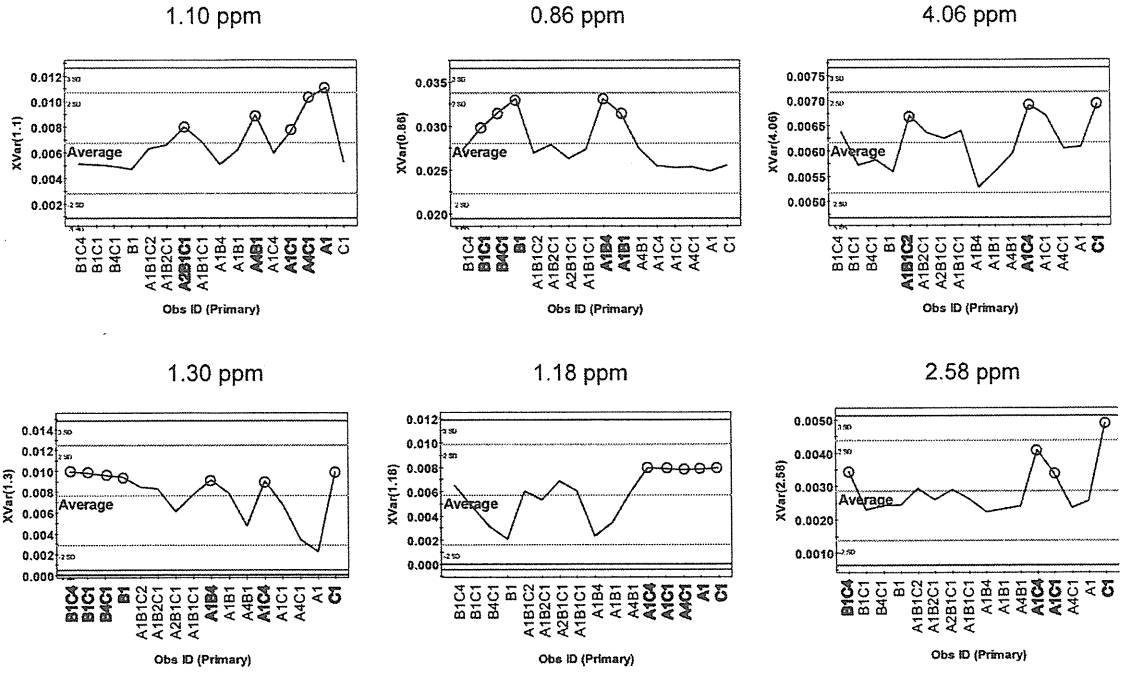

Fig. 5. The PCA Trend Plot: Integrated Intensities of Six Variables Showing Typical Fluctuations of Human Insulin, Bovine Insulin, and Porcine Insulin on the Loading Plot

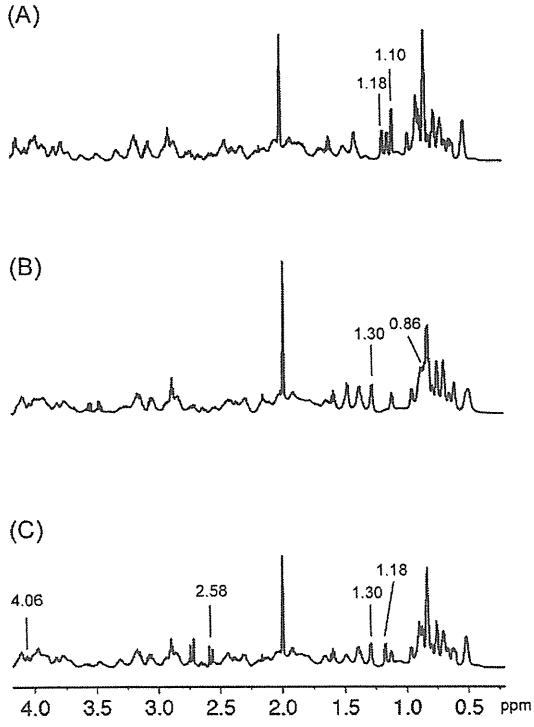

Fig. 6. The Typical Chemical Shifts for the Different Insulin Species on the PCA Loading Plot: Human (A), Bovine (B), and Porcine (C)

insulin, as shown in Fig. 4.

Discussion

The three insulin species used in this study each consist of 51 amino acid residues; bovine insulin has three different positions and porcine insulin has one different position from human insulin. In general, it is extremely difficult to distinguish differences of one to three amino acid residues in the ^{1}H-NMR spectrum of polypeptides of approximately MW 6000. However, we succeeded in distinguishing between the insulin species using a combination of multivariate statistics and ^{1}H-NMR spectra. PCA of the insulin spectrum for each mixture ratio was performed, and variables due to several different amino acid residues were detected from both the scores of PC1 and PC2, clearly depicting three separate groups, as shown in Figs. 3 and 4. In addition, from the scores plot, the components of the single insulin species and of mixtures consisting of two-three species were statistically distributed in the triangular phase diagram according to differences in the species composition ratio (Fig. 3, Table 1). This result shows that it is possible to analyze the composition of a mixture of species with a small number of amino acid sequence differences by taking advantage of the scores plot.

We also examined by PCA the partial aliphatic and amide regions of each insulin spectrum (data not shown). The determination of the variables contributing significantly to the variation of the PC1 coordinate axis for the human and bovine insulin groups and to the variation of the PC2 coordinate axis for the two groups, porcine, and both human and bovine insulin groups of the loading plots was performed by analysis of the amino acid residue peaks corresponding to these particular variables. Differences of the characteristic amino acid residues for each insulin species as well as the results from analyzing entire spectra were reflected in the scores plot. It is noteworthy that a similar tendency from analysis of the complete spectral region was observed with the scores plot of the amide region. These results suggest that it may be possible to distinguish slight sequence differences of polypeptides by PCA analysis of the amide region of the NMR spectrum.

On the other hand, the biological effect of polypeptides is also influenced by differences in their higher-order structure. It is difficult to evaluate differences in the higher-order structure of polypeptides by conventional analytical methods. In this PCA analysis study, it was found that the first and second principal components accounted for a majority of the vari-

ability differences of the primary insulin species structures. Interestingly, there were some variables that were not derived from the differences of amino acids among the three insulin types. Through a comparison of the NOESY spectra of the insulin species, it was proposed that these variables were associated with differences in the higher-order structures (data not shown). Therefore, the NMR technique coupled with PCA might also be useful as a tool for analyzing the higher-order structure, which is associated with the quality of a polypeptide, because in addition to primary structure information of the amino acid residues, the ^{1}H-NMR spectrum also contains information related to the three-dimensional structure of a molecule that is dependent on the solution conformation.

In conclusion, we have succeeded in precisely characterizing samples of human, bovine, and porcine insulin, molecules that differ in amino acid sequence from one to three amino acid residues, by ^{1}H-NMR spectroscopy coupled with PCA. Currently, assessment of the differences of higher-order structure using PCA analysis of NOESY spectral data are underway.

Acknowledgements We thank Dr. J. Kurita and Mr. K. Kushida (Agilent Technologies Japan Ltd.) for their technical assistance in measuring the NMR spectra. This work was supported by a Health Labour Sciences Research Grant from the Ministry of Health, Labour, and Welfare, Japan and by a 'Grant-in-Aid for Young Scientists (B)' (No. 22790126) from the Ministry of Education, Culture, Sports, Science and Technology (MEXT) of Japan.

References

1) Eriksson L., Johansson E., Kettaneh-Wold N., Wold S., "Multi- and Megavariate Data Analysis," Umetrics Academy, Umeå, 2001.
2) Wold S., Albano C., Dunn W. J., Edlund U., Esbensen K., Geladi P., Hellburg S., Johansson E., Lindberg W., Sjostrom M., "Chemometrics: Mathematics and Statistics in Chemistry," D. Reidel Publishing Company, Dordrecht, 1984.
3) Clayton T. A., Baker D., Lindon J. C., Everett J. R., Nicholson J. K., *Proc. Natl. Acad. Sci. U.S.A.*, **106**, 14728—14733 (2009).
4) Clayton T. A., Lindon J. C., Cloarec O., Antti H., Charuel C., Hanton G., Provost J. P., Le Net J. L., Baker D., Walley R. J., Everett J. R., Nicholson J. K., *Nature* (London), **440**, 1073—1077 (2006).
5) Coen M., Holmes E., Lindon J. C., Nicholson J. K., *Chem. Res. Toxicol.*, **21**, 9—27 (2008).
6) Crockford D. J., Holmes E., Lindon J. C., Plumb R. S., Zirah S., Bruce S. J., Rainville P., Stumpf C. L., Nicholson J. K., *Anal. Chem.*, **78**, 363—371 (2006).
7) Fukuhara K., Ohno A., Ando Y., Yamoto T., Okuda H., *Drug Metab. Pharmacokinet.*, **26**, 399—406 (2011).
8) Ohno A., Kawasaki N., Fukuhara K., Okuda H., Yamaguchi T., *Chem. Pharm. Bull.*, **57**, 1396—1399 (2009).
9) Ohno A., Oka K., Sakuma C., Okuda H., Fukuhara K., *J. Agric. Food Chem.*, **59**, 5181—5187 (2011).
10) Pongsuwan W., Bamba T., Yonetani T., Kobayashi A., Fukusaki E., *J. Agric. Food Chem.*, **56**, 744—750 (2008).
11) Uchiyama M., Toyoshima S., Ono S., Uyama Y., "Iyakuhin Hyouka Gaisetu," Tokyo Kagaku Doujin, Tokyo, 2009.
12) Ohno A., Kawasaki N., Fukuhara K., Okuda H., Yamaguchi T., *Magn. Reson. Chem.*, **48**, 168—172 (2010).
13) Bocian W., Sitkowski J., Bednarek E., Tarnowska A., Kawecki R., Kozerski L., *J. Biomol. NMR*, **40**, 55—64 (2008).
14) Nicholson J. K., Foxall P. J., Spraul M., Farrant R. D., Lindon J. C., *Anal. Chem.*, **67**, 793—811 (1995).

特集
PATの現状と展望
1

PATによる医薬品品質管理の課題と展望

Perspective on PAT in Pharmaceutical Quality Control

国立医薬品食品衛生研究所 薬品部
小出達夫，香取典子，檜山行雄，奥田晴宏
TATSUO KOIDE, NORIKO KATORI, YUKIO HIYAMA, HARUHIRO OKUDA
Division of Drugs, National Institute of Health Sciences

はじめに

PAT（Process Analytical Technology）は，「最終製品の品質保証を目標として原材料や中間製品／中間体の重要な品質や性能特性及び工程を適時に（すなわち製造中に）計測することによって，製造の設計，解析，管理を行うシステム」（ICH Q8（R2）ガイドラインより）である。PATは2002年のFDAの「Pharmaceutical Current Good Manufacturing Practices（cGMPs）for the 21st Century: A Risk-Based Approach」に取り上げられたころから，日本でも注目されるようになった。現在ではQbD（Quality by Design）アプローチを行うための重要なツールの１つとして製剤開発，製造工程管理に活用されるようになったが，これまでに実際にPATを医薬品品質管理に採り入れていく過程においてさまざまな問題点が浮かび上がってきた。そこで本稿ではPATによる医薬品品質管理における課題および展望について記述する。

1．医薬品品質保証のパラダイムシフトとPATの必要性

医薬品の品質保証は，遠い昔は出荷時の品質試験のみによるものであった。そのため製品の品質のばらつきが大きい場合では数少ないサンプル数，例えばN=３の品質試験では不良品が試験をすり抜け出荷されてしまう確率が非常に高くなってしまうため，品質保証のレベルが非常に低いと言わざるを得なかった。1970年代からは徐々にGMPやバリデーションの考え方が医薬品製造管理に導入され，製造工程を管理することにより品質のばらつきが抑えられることとなり，出荷試験のみの場合と比べて品質保証のレベルは向上していくこととなった。そして21世紀に入ると，製剤開発にQbDアプローチを採用することで製剤設計の段階でばらつきの少ない一定の品質を持つ製品を作ることができるように設計することがICH Q8ガイドライン等において推奨されたため，今後，品質保証のレベルがさらに向上していくと考えられる。実際に最近では多くの企業が品質保証の向上を目指して製剤開発にQbDアプローチを採り入れるようになってきている。

このようにこれからの医薬品の品質保証は，品質試験，製造管理，そして製剤設計の３つの要素から構成されるようになると考えられ，そのため製剤開発におけるQbDアプローチの必要性およびその関連する研究はますます重要度が高まると考えられる。QbDはQ8ガイドラインにおいて「事前の目標設定に始まり，製品及び工程の理解並びに工程管理に重点をおいた，立証された科学及び品質リスクマネジメントに基づく体系的な開発手法」と定義されており，このような体系的な開発をするためには効率的なプロセス理解および工程管理が行えるPATのような技術が必要となる。さらにはPATにより工程内で品質管理が可能になれば最終の品質試験は不要になるのでは，という考えからRTRT（Real Time Release Testing：リアルタイムリリース試験）という新たな品質管理の手法が出てきたことなど，医薬品の品質管理手法は大きな変革期を迎えており，現在，PATの重要性が非常に高まっている。

2. PATの医薬品品質管理への応用と問題点

PATの医薬品品質管理への応用としては，PATを単なる工程のモニタリングや工程内試験のみに用いる場合（最終の品質試験を出荷試験とする）と，PATを出荷試験のデータとして用いるRTRTに用いる場合の２通りに分けられ，それぞれ品質管理における現状が異なっている。RTRTはICH Q8（R2）において「工程内データに基づいて，工程内製品及び／又は最終試験の品質を評価し，その品質が許容されることを保証できること。通常，あらかじめ評価されている物質（中間製品）特性と工程管理との妥当な組み合せが含まれる」と定義されており，最終の品質試験を行わないのはスキップテストと同じであるが，スキップテストのようにまったく試験を行わずに出荷するのではなく，工程内でCQA（Critical Quality Attribute：重要品質特性）等を測定，評価した結果をもって出荷試験としている。そのためPATを用いたRTRTを行う場合は，PATを単なる工程内試験のみに用いる場合とは異なり，工程内試験法およびその管理値を最終品質試験方法およびその規格値と同等に取り扱う必要性が生じた。また，RTRTを採用しても安定性試験や代替試験法として最終品質試験を設定しておく必要があると考えられるので，最終品質試験による管理とRTRTによる管理を共存させる必要性が出てきた。これらのことからPATをRTRTに用いる場合の，最終品質試験による管理とRTRTによる管理との整合性について新たな規制上のルールを作り上げることが現在，課題となっている。

その一例として，これまでにほとんど最終品質試験に用いられていなかったNIR（近赤外分光法）を用いたPATによるRTRTにおける試験法のルールづくりがあげられる。特にNIRを定量試験として採用する場合，多変量解析という特殊な手法を使うことが多くなるため，検量線を作成する（キャリブレーション）手法および検証する（バリデーション）手法，構築したシステムが試験前に正しく動いていることを確認する方法（システムの性能）について，これまでのHPLCなどの定量に用いられてきた設定方法とは異なる方法が要求される。さらにNIRは測定データが温度，湿度等の環境や粒子径や密度などの物性等多くの要因に左右され，その上開発時にこれらの要因がすべて検量線に反映されているとは限らないため，開発時に組み込まれなかった何らかの要因により検量線にずれが生じていないか継続的に確認するための定期的な点検（定期再バリデーション）を行う際のルールを必要とする（ただし試験方法により一部不要の場合もある）。しかしNIRという手法自体が複雑で多くの場合個々の状況に応じた柔軟な対応が必要となるため，その妥当性を一律に判断してルールを決めておくことは非常に難しい。

また，NIRのようなPATを用いたRTRTは含量均一試験などに適用が想定されるが，一般的に用いられるHPLCなどによる定量による局方試験とNIRによるRTRTでは分析法自体が異なるため，これまでの局方試験と同じ判定基準をRTRTにそのまま用いることができない。そのため，PATを用いたRTRTの規格値の妥当性および局方試験法との整合性を考慮する必要が生じている。例えば，局方の含量均一試験ではサンプルサイズが10～30錠で１回の試験が行われるが，NIRなどのPATを用いる場合では何百～何千錠で試験を行うことになり，サンプル数が異なるため局方と同じ基準を使うことは難しい。PATを用いたRTRTの場合にはサンプルサイズが限られている薬局方の試験規格をそのまま準用することを考えるよりも，母集団の特性に応じた試験規格を，薬局方の許容品質を保持しながら規定することが望ましいと考えられる。この含量均一試験の問題については欧米ではLarge N法およびその改法など[1~4]が対応策として提案されている。

以上の課題を例にあげてきたが，これらの運用上の問題の解決については，ICHのIWG（Implementation Working Group：Q８，９，10についての実施に関する作業部会）のQ&AやPoints to Consider，また日本においてはサクラ錠Mockおよびその報告書[5,6]に方針が示されている。また厚生労働科学研究においてもさらなる議論が続いており，近くその内容が公開される予定である。これらの情報については国立医薬品食品衛生研究所薬品部のウェブサイト（http://www.nihs.go.jp/drug/DrugDiv-J.html）や本誌等で順次，提供される予定である。

3. PATの発展についての展望

前項で示したようにPATは課題も多いが，品質管理に使う上では非常に有用な手法であるため，原薬合成，造粒，乾燥，打錠等，さまざまな工程において，NIRやラマンなど多くの分析法により行われており，その応用

はさらに発展すると考えられる。そこで，今取り組まれているPATの応用についての展望をこの項で記述したい。

(1) SustainabilityにおけるPATの活用

有機溶媒使用量の削減を念頭に置いたIn-line GC-MSによる原薬製造工程中の有機溶媒量のコントロールや，有機溶媒を用いるHPLCのような最終試験から溶媒を用いないNIRなどの分光学系試験もしくはRTRTへの転換など，PATの活用およびRTRTの採用が検討されている[7]。このような環境，エネルギー問題など，いわゆるグリーンイノベーションの観点からもPATは有望視されている。

(2) Continuous Manufacturing Processへの適用

欧米では近年Continuous Manufacturing Process（連続工程）の導入により，製造工程を一体化することが検討されている。そのメリットとして場所，時間，原料等の資源の節約ができ，また開発時のスケールアップ問題の解消にも繋がるため，製剤開発が明確かつ迅速に行われるようになるということがあげられる。しかし連続工程においては試験におけるサンプリングを製造ロット，バッチ単位から時間単位などに変えるなどの対応が必要となる。そのため連続測定が可能なPATやそれを用いたRTRTとContinuous Manufacturing Processとの組合せによる品質管理は非常に相性の良い手法である。米国FDAもこのような革新技術の導入への取り組みに対してシンポジウム等[8]で支持を表明しており，そのため今後，PATが活躍する場はますます増えると考えられる。

(3) 新しいPAT技術としてのラマン分光法

NIRはPATとして最も実用化が進んでいる分析技術であるが，温度，湿度などの外部環境や粒子径など原料の物性に測定結果が影響される，NIRによる測定が不可能な化合物もあり，また多変量解析を用いることから解析を理解することが難しい，さらには検量線のメンテナンス等に手間がかかるため問題点が多い。そのため研究レベルではあるが前方散乱型（透過型）ラマン[9]のような新しいPAT技術の開発，導入の検討が積極的に行われている。ラマン分光法はこれまで後方散乱型（反射型）が主であったが，前方散乱型ラマン分光法を導入することができれば錠剤等が精度良く解析，定量できるようになり，また検量線のメンテナンスが不要になる等，NIRより解析が簡素化できるため次世代のPATの実用化技術として有望視されている。

(4) 製剤のイメージング技術の利用

NIRやラマン等を用いた製剤のイメージング技術は製剤中の物理的もしくは化学的情報を視覚化するため，製造中に何がどのように起きたのかを把握することができ，PATのみを用いた場合と比べて製剤および製造工程の理解が高まりやすい。その活用の一例を**図1**に示す。A，Bの２種類の製剤があり，NIRイメージングのデータから製剤Aは錠剤中の主薬が均一のため，NIRを用いたPAT，RTRTで定量を行う場合，透過でも反射でも測定できる。一方，製剤Bでは表面と内部の主薬量が異なり，不均一なために透過測定しかできない。また主薬分布が不均一なため測定のばらつきが大きくなる原因となることも考えられる。このようにイメージング技術を併用することにより製剤に対する理解が高まり，適切なPATの導入に繋がる。またイメージング技術は単独でも混合均一性評価などのPATとして活用できる[10]ので，今後応用がさらに発展すると考えられる技術である。

筆者の研究グループは，高度分析評価技術を応用した医薬品製剤開発および製造工程管理手法をテーマに，PATに用いられる先進分析技術および顕微分光イメージング技術の評価研究や，これらの技術の製剤開発およ

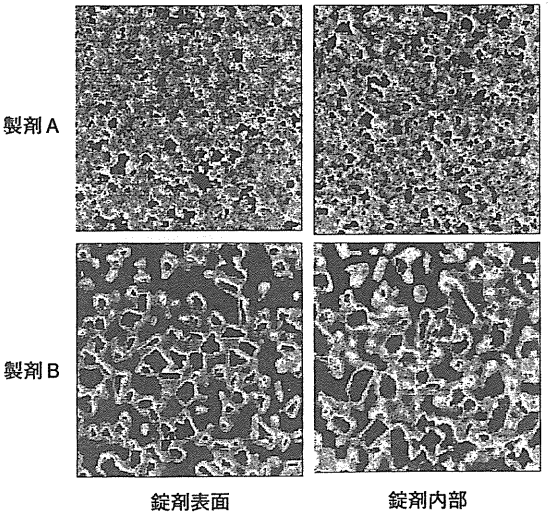

図1　NIRイメージング技術の応用例
製剤Aでは表面および内部の主薬量（イメージ中の赤い部分）はほぼ同一（50%）であるが，製剤Bでは主薬量は表面では約40%で内部では60%と大きな差があり，錠剤内部に主薬が偏析して不均一になっていると考えられる。

び製造工程管理への応用研究を産官学の共同研究として行っている。本研究については不定期ではあるが1～2年に1度，研究発表会を開催して情報提供を行っている。

4. A QbD(Analytical QbD)について

QbDは製剤開発に使われるアプローチであるが，近年，このQbDの考え方を分析手法の開発アプローチに応用する取組みがある。通常，QbDアプローチの手順は，目標製品品質プロファイルの設定に始まり，経験，知識やこれらを生かしたリスクマネジメント，開発研究における実験結果を組み合わせた検討よりCQAを特定して，CQAと物質特性および工程パラメータとの関連づけから製造工程の理解を行い，製造工程および品質保証のための最終的な管理戦略を構築する。分析手法の開発は通常管理戦略中に行われるが，A QbDによるアプローチの場合，同じように最初に何をどのように測定するか分析標的プロファイルを決める，そして測定方法の選択，測定法に影響する要因，例えば温度，湿度等のリスク評価，要因を把握することにより分析法の理解を行い，その分析法における頑健性のデザインスペースを設定する等管理戦略を構築するという，製剤開発の場合とほぼ同じような手順を踏むことになる。その枠組みを**図2**に示す。このようなA QbDアプローチを導入することにより頑健な分析法が開発され，その割合が増加したという報告[11]もある。またPATは今後新しい分析技術が開発されると考えられるため，新しい分析手法の開発の際にA QbDが開発アプローチの1つとなり得ると思われる。もちろん，A QbDは通常のHPLCなどの分析法開発にも応用が可能である。これからの分析法開発はリスクマネジメントを導入していくことにより，N=3から科学とリスクをベースとした品質管理へ移行した製剤開発のQbDのように，6σによる管理基準から科学とリスクをベースとした管理基準による分析法開発へと移行していくと考えられる。

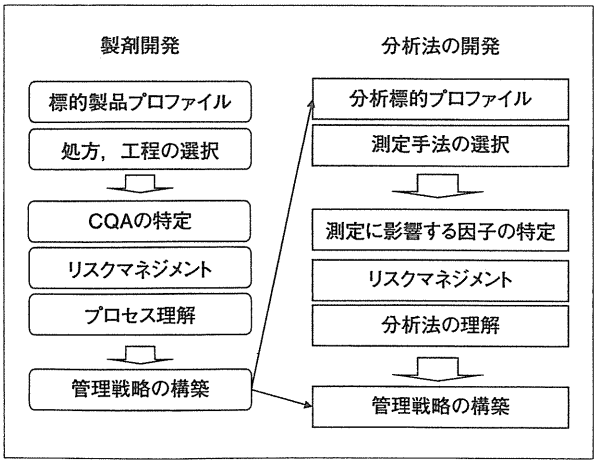

図2　QbDとA QbDの比較

おわりに

これからの医薬品品質保証において最も重要視される点は，科学的根拠に基づく製品の理解および適切な品質管理戦略の構築である。PATは，まだ課題が多く残っているが，科学的根拠に基づいて製造工程を理解し，それをコントロールする技術としてこれからも重要な役割を果たしていくと考えられる。そしてPATの活用により，科学的な根拠に基づく品質管理技術が発展し，品質の良い医薬品の安定な供給に役立つと考えられる。

■参考文献
1) D. Sandell, K. Vukovinsky, M. Diener, J. Hofer, J. Pazdan, J. Timmermans：Development of a Content Uniformity Test Suitable for Large Sample Sizes, Drug Information Journal, **40**, 337-344(2006)
2) J. Bergum, K. E. Vukovinsky：A Proposed Content Uniformity Test for Large Sample Sizes, Pharmaceutical Technology, Nov 2, 72-79(2010)
3) Demonstration of Uniformity of Dosage Units Using Large Sample Sizes, Proposal for a new general chapter in the European Pharmacopoeia, Pharmeuropa, **23**(2), 285-293(2011)
4) Y. Tsong, M. Shen：Parametric two-stage sequential quality assurance test of dose content uniformity, Journal of biopharmaceutical statistics, **17**(1), 143-57(2007)
5) 檜山行雄：原薬・製剤開発研究に基づいた製造・品質管理手法の研究－重要工程におけるデザインスペース及びControl StrategyとしてのReal Time Release等の研究 分担研究報告書(2008)
6) 檜山行雄：医薬品の製造開発から市販後に及ぶ品質確保と改善に関する研究－製剤の開発・製造情報に関する研究 分担研究報告書(2010)
7) Sustainability and PAT applications, 37th FACSS Symposium(2010)
8) C. Moore：Regulatory Perspective on Continuous Manufacturing, AAPS Annual Meeting Symposium(2010)
9) C. Eliasson, N. A. Macleod, P. Matousek, L. C. Jayes, F. C. Clarke, S. V. Hammond, M. R. Smith：Rapid non-invasive quantitative assessment of pharmaceutical capsules using transmission Raman spectroscopy, CENTRAL LASER FACILITY ANNUAL REPORT, 256-259(2007/2008)
10) A. S. El-hagrasy, H. R. Morris, F. D'Amico, R. A. Lodder, J. K. Drennen Ⅲ, Near-infrared spectroscopy and imaging for the monitoring of powder blend homogeneity, J. Pharm. Sci, **90**(9), 1298-1307(2001)
11) J. F. McCafferty, P. Nethercote：Applying QbD Approaches to Analytical Methods, AAPS Annual Meeting Symposium(2011)